Journal of
Materials Chemistry C

REVIEW

View Article Online
View Journal | View Issue

Open Access Article. Published on 17 2023. Downloaded on 05.11.2024 09:24:16.
This article is licensed under a Creative Commons Attribution-NonCommercial 3.0 Unported Licence.

Cite this: *J. Mater. Chem. C*, 2023, **11**, 3162

Review of photocathodes for electron beam sources in particle accelerators

Jana Schaber, *[ab] Rong Xiang [a] and Nikolai Gaponik [b]

Received 4th September 2022,
Accepted 4th February 2023

DOI: 10.1039/d2tc03729g

rsc.li/materials-c

This paper compares different photocathodes that are applicable for electron injector systems and summarizes the development in cathode technology in the last years. The photocathode is one of the key components of the facilities that provides electrons for many research experiments. Typically, a high efficiency and a long operation time are desired, thus the photocathode needs to be robust against any rest gases occasionally available during operation. Low thermal emittance and fast response time are special requirements for the accelerator community. These parameters are commonly used to compare the various cathode materials. Metals and plasmon-enhanced materials emit electrons from the near surface, whereas semiconductors emit photoelectrons mostly from the bulk region. We compare metal photocathodes such as magnesium, copper and lead, with semiconductor photocathodes such as cesium telluride, antimonide photocathodes and III–V semiconductor photocathodes. GaAs and its typical application for the generation of spin-polarized electrons is discussed and special attention has been paid to the emerging GaN as a potential novel photocathode. The above mentioned state-of-the-art cathodes are compared regarding their preparation approaches, quantum efficiency, lifetime, response time and their status of application. This work is aimed to provide a guideline for particle accelerator researchers in their choice of the cathode material. Thermionic cathodes and field emission cathodes are not discussed in this review.

1 Introduction

Electron sources represent a key component in modern technologies such as microscopes,[1–3] radio transmitters,[4] and X-ray tubes for medical diagnostic devices.[5] A wide range of applications is covered by the ability to accelerate electrons in a particle accelerator. The development of a better electron source is crucial for both fundamental and applied research. The improvement of the existing electron sources is directly linked to strong demands on higher electron currents, higher repetition rates or high brightness beams.[6,7]

In the last decades, the development in accelerator technology contributed to advanced cancer diagnostic and therapy,[8] and helped to understand chemical reaction mechanisms[9] and molecular excitation and vibration states.[10] Free electron laser (FEL), especially X-ray free electron laser (XFEL) facilities[11,12] and terahertz (THz) radiation sources[13] are powerful tools with a wide application in biomedicine, security imaging and condensed matter physics. These tools require high brightness electron beams that are generated from so-called photocathodes inside a photoinjector.

The principle of an accelerator electron source begins with the generation of electrons and the subsequent acceleration of those downstream. The electrons are accelerated away from the cathode by an electric field, and afterwards they are collimated to form a compact electron bunch. A vacuum environment protects the cathode from toxic contaminations and prevents electron scattering on gas molecules or residual particles.

In accordance to the nature of the electric field applied to the cathode, accelerator facilities can be distinguished into three different injector types.[14–16] One possibility is to apply a direct current (DC) electric field between cathode and anode. Depending on the applied DC field, the electrons gain energies between 100–500 kV. A disadvantage of DC electron sources is that electrons are not accelerated to relativistic energies. Such DC electron sources are used in Cornell Laboratory for Accelerator-Based Science and Education (CLASSE),[17] National Laboratory for High Energy Physics (KEK)[18] and Microtron Accelerator Mainz (MAMI).[19]

Another possibility instead of a DC field is the application of a radio-frequency (RF) field. In RF injectors the cathode is surrounded by a special shaped resonance cavity. Thus, no anode is needed. Deutsches Synchrotron (DESY),[20] European Organization for Nuclear Research (CERN)[21] and Paul-Scheerer Institute (PSI)[22] use such RF injector systems.

[a] Helmholtz-Zentrum Dresden-Rossendorf, Bautzner Landstraße 400, 01328 Dresden, Saxony, Germany. E-mail: j.schaber@hzdr.de
[b] Technische Universität Dresden, Helmholtzstr. 10, 01069 Dresden, Saxony, Germany

This journal is © The Royal Society of Chemistry 2023

Open Access Article. Published on 17 2023. Downloaded on 05.11.2024 09:24:16.
This article is licensed under a Creative Commons Attribution-NonCommercial 3.0 Unported Licence.

A special type of RF technology is used in the superconductive radio-frequency (SRF) injector. It also has a resonance cavity, made of niobium (Nb) which allows a superconducting state at very low temperatures. Therefore, the Nb cavity has to be cooled constantly at a cryogenic temperature to guarantee this superconductivity. SRF injectors are used for example at ELBE[23] and at Brookhaven National Lab (BNL).[24]

As mentioned, the cathode is the origin of the generated electrons and can be a metal, including plasmon-enhanced materials, or a semiconductor. An energy source is necessary to excite electrons above the work function with the desired consequence of the emission of cathodic electrons. The necessary energy can be supplied either thermally, with an electric field or with photons. The thermionic and the field emission are the mature methods and work robustly. However, the photoemission offers more advantages, for example that the electron bunches can be time structured.

The choice of suitable cathodes for high brightness electron beams depends on many factors. A perfect photocathode should provide a high quantum efficiency (QE) at convenient laser wavelength, long lifetime, fast response time and low thermal emittance. Especially, the criterion of high QE has an extraordinary importance and can not be fulfilled by the existing photocathodes.[25] For example, none of these known cathodes can provide such high QE to meet a high beam current as it is required for future energy recovery lines (ERL) applications.[26–28]

The development of better photocathodes is progressing steadily and rapidly. Metal cathodes such as copper (Cu), magnesium (Mg) and lead (Pb) are used as the first cathodes when an accelerator facility is commissioned. But the fast development of the particle accelerator devices and the strong desire to achieve higher bunch charges and currents leads to the usage of semiconductor photocathodes such as cesium telluride (Cs_2Te), alkali antimonide (K_2CsSb) or gallium arsenide (GaAs). In the last decades, an intensive research on GaAs led into the field of III–V semiconductors and especially gallium nitride (GaN) was identified to be a promising photocathode for future high current applications in the particle accelerator field.

In SRF Guns the right choice of the photocathode is extremely relevant, because the cavity is sensitive to any contamination. This risk is the potential release of the photocathode components into the cavity and its re-deposition at high field regions. Furthermore, the prevention of a potential overheating of the photocathode is the next considerable point. A proper thermal contact is crucial to avoid a cathode overheating, that is caused by laser irradiation and RF dissipation. One possibility for the heat dissipation is to conduct it into a liquid helium environment of the cavity. Another possibility represents the non-contact cathode, which requires an external cooling. In the non-contact mode, the biggest advantage is that the cathode can be operated at temperatures different from the cavity temperature.[29]

In this review, we introduce the requirements for high current electron beams and discuss different photocathodes regarding to their quality and performance. We compare metal photocathodes with semiconductor photocathodes and give an outlook on the potential use of III–V semiconductors, especially GaN as a considerable photocathode.

2 Requirements for high current electron beams

In the following section the requirements for high current electron beams and fundamental key terms are described. Fulfilling the desired requirements such as QE, long lifetime, low dark current, low thermal emittance and fast response time lead to the promising developments in the field of semiconductor photocathodes.[25,30,31]

2.1 Quantum efficiency (QE)

QE is one of the most important parameters, when dealing with photocathodes. QE is defined by the ratio of the number of generated photoelectrons divided by the number of incident photons,[7] as shown in eqn (1). The QE can be more practically calculated by the ratio of h (Planck constant), c (speed of light) and I (measured photocurrent from the photocathode) to q_e (elementary charge of an electron), λ (incident wavelength) and P_{light} (power of incident light), also shown in eqn (1).

$$\mathrm{QE} = \frac{N_{\mathrm{electrons}}}{N_{\mathrm{photons}}} = \frac{h \cdot c}{q_{\mathrm{e}}} \mathrm{x} \frac{I}{\lambda \cdot P_{\mathrm{light}}} \quad (1)$$

Therefore, a maximum QE is achieved by a minimum laser power and a maximum photocurrent.

The electronic structure of an emissive material and its relation to the outside environment are characterized by many key terms. An overview of these key terms such as work function, electron affinity and Fermi level (E_{Fermi}) has been summarized in Fig. 1 to convey the basic principles of a photocathode.[32]

The electronic structure of the material surface differs from sample to sample, caused by many internal and external factors such as lattice structure, material defects, morphology and surface composition, especially its surface cleanness. As shown in Fig. 1, the energy levels of electron transport are defined as conduction band (CB) and valence band (VB). The conduction band minimum (CBM) represents the lowest energy level of the unoccupied state of the uncorrelated electron and quasi-electrons. In contrast the valence band maximum (VBM) is the highest energy level of occupied states with correlated electrons. The energy difference between these two levels is called band gap (E_{gap}). The E_{Fermi} is the highest occupied level where electrons are flexible and can move around freely. Therefore, E_{Fermi} marks the boundary between occupied and unoccupied states in a continuum of states.

A vacuum energy barrier (E_{vac}) prevents flexible electrons from escaping from the materials surface. Thus, E_{vac} defines the potential energy of an electron positioned in a space outside of the solid. The E_{vac} location is strongly influenced by the nature of the material surface.

Open Access Article. Published on 17 2023. Downloaded on 05.11.2024 09:24:16.
This article is licensed under a Creative Commons Attribution-NonCommercial 3.0 Unported Licence.

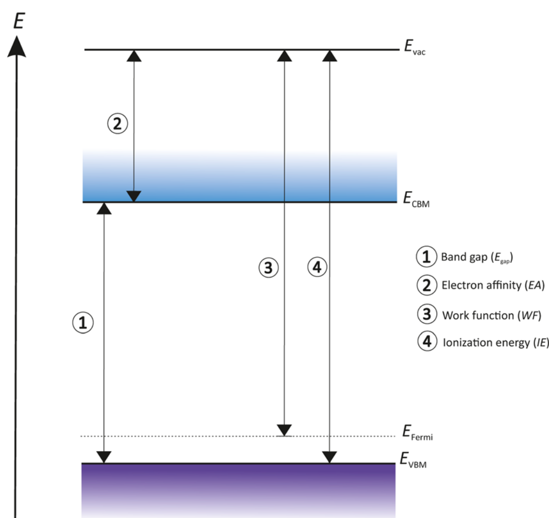

Fig. 1 Schematic representation of the fundamental key terms in photoemission processes.

The energy difference between E_{vac} and VBM is defined as ionization energy (IE) and characterizes the minimum energy needed to remove an electron out of the material. Whereas the electron affinity (EA) is the energy difference from E_{vac} to CBM.

The work function (WF) is the necessary energy to remove an unbounded electron from E_{Fermi} and place it outside of the surface in free space.

For semiconductors the work function depends on E_{Fermi}, influenced by the density of states, temperature and carrier concentration. The work function prevents a free electron at E_{Fermi} to escape from the solid into the outside space, and the work function is influenced by two main components, namely a bulk component (electronic density of states in the solid) and a surface component (redistribution of charges at the surface). A redistribution of the electron density can occur which is a consequence of coulomb repulsion and Pauli exclusion from adsorbates on the surface. Any deposition of an electronegative adsorbate on the surface results in an electron transfer that increases a surface dipole and influences the related surface terms.

2.2 Thermal emittance and mean transverse energy (MTE)

Thermal emittance is an important key factor for the maximum achievable electron brightness, depending on the electron source. Thermal or intrinsic emittance describes the transverse momentum of emitted electrons from the material surface. It considers the cathode material, its surface quality (roughness and crystallinity), the applied electric field and the incident laser wavelength.[33] Therefore, thermal emittance includes all the physics in the emission process and the cathode material properties and summarizes the divergence of the cathode emittance.[25] The thermal emittance also depends on the Mean Transverse Energy (MTE) of electrons. MTE does not depend on the spot size of the drive laser, but reflects the properties of the cathode material, the cathode surface condition[34–36] and the drive photon energy.[37] Thus, MTE is also an important parameter for describing the cathode properties. The electric field on the surface, the crystal defects inside the semiconductor cathode,[38] and the operation temperature[25] have an influence on the MTE as well.

Eqn (2) shows a widely used formula to describe the thermal emittance.[7] Often different formulas are given considering even more emission parameters such as E_{gap}, electron affinity or photon energy.

$$\varepsilon_{n,\mathrm{rms,thermal}} = \sigma_{\mathrm{laser,rms}}\sqrt{\frac{kT_\perp}{m_\mathrm{e}c^2}} = \sigma_\mathrm{X}\sqrt{\frac{\mathrm{MTE}}{m_\mathrm{e}c^2}} \qquad (2)$$

$\sigma_{laser,rms}$ is the root mean square (rms) spot size of the laser and c the speed of light in vacuum. $kT_\perp$ means the electrons effective transverse energy, m_e the electron mass and σ_X, and MTE are the rms size of the electron bunch, starting from the cathode, and the mean transverse energy of the electron beam, respectively. $kT_\perp$ will approach the crystal lattice temperature when the photocathode is illuminated with a photon energy near its E_{gap}. For GaAs, as a negative electron affinity (NEA) photocathode, $kT_\perp$ is 25 meV at room temperature. If the wavelength is greater than the E_{gap}, the effective temperature of the electrons increases. For non NEA cathodes the effective temperature is always above the cathodes temperature.[25]

In fact, for photocathodes a low thermal emittance is desirable and typical values are between 0.5–1.5 μm, depending on the cathode material.

2.3 Lifetime

The photocathodes lifetime and its performance are determined by many factors, but especially by the vacuum conditions. All of the known photocathodes require an ultra-high vacuum (UHV) environment to provide a sufficient QE and lifetime. Photocathodes are influenced immediately by any residual gases inside the UHV system. Surface poisoning and the related efficiency loss were studied and reported for metal cathodes exposed to gases for longer time.[39] However, for metal photocathodes the adsorption of residual gases is typically less significant than for semiconductors. Semiconductors such as Cs_2Te or GaAs are immediately influenced by any vacuum instabilities.[40,41] The photocathode surface is contaminated by the adsorption of residual gas or molecules, leading to the increase of the electron affinity and obstructing the ejection of photoelectrons into the vacuum. The photoemissive cathode might also react with the residual gas molecule, leading to a band structure change. Therefore, it is necessary to keep the pressure as low as possible with the help of suitable vacuum pumps for UHV application (ion pumps and non-evaporable getter (NEG) pumps). The combination of these pumps can guarantee a vacuum between 10^{-10}–10^{-11} mbar. Especially GaAs is highly sensitive to any residual gases and requires minimum 10^{-11} mbar or better vacuum.

2.4 Dark current

Dark current means the unwanted electron emission in photoinjector systems.[42,43] The main sources for field emission are

Open Access Article. Published on 17 2023. Downloaded on 05.11.2024 09:24:16.
This article is licensed under a Creative Commons Attribution-NonCommercial 3.0 Unported Licence.

the photocathode itself and/or the cavity behind the photocathode. Undesired electrons are hazardous to the components downstream and have to be sorted out. It is crucial to discover the source location in order to prevent possible damage on the accelerator components.

$$i = (\beta \cdot E)^{5/2} \cdot \mathrm{e}^{-\frac{B}{\beta \cdot E}} \quad (3)$$

The undesired field emission is characterized by the Fowler–Nordheim relation to describe the current density,[42,44] shown in eqn (3). E is the electric field, B is a material depended parameter and β is the field enhancement factor, depending on the emitters geometry. This relation fits best to metallic emitters but can be applied also to semiconductor materials. The sources for dark current are usually irregularities on the photocathode surface which appear as macroscopic tips, needles or particles. Exposed to the electric field, these surface irregularities cause a high β.[43,45] Thus, it is necessary to provide a smooth and particle-free surface before an RF field is applied to the cathode.

Scanning electron microscopic (SEM) and atomic force microscopy (AFM) are useful tools to characterize the surface structure and the roughness. Both techniques are widely used and detectable breakdown spots in the cathode surface are identified as a reason for the strong emission.[43] Small irregularities in the grain boundaries and defects in the crystal structure are also assumed to cause strong emission. The best way to minimize surface irregularities is to use a polished mirror-like materials of high-crystal quality.[44]

2.5 Response time

An important parameter for the generation of short electron pulses in less than picosecond (ps) regime is response time.[7]

Response time means the total time elapsed between the excitation of the electrons by incident photons, their tunneling towards the surface and their final escape from the cathode surface into the vacuum.[25] Photosensitive materials with a longer response time are not considered to be a photocathode in particle accelerators because of their temporal spread. Thus, a complex bunching and chopping downstream of the electron beam path would be necessary. Recent measurements of Cs_2Te, tri-cesioantimony (Cs_3Sb) and GaN photocathodes show prompt response in femtosecond (fs) regime. Response time can be diagnosed with a deflecting cavity synchronized to a laser pulse train.[30,46,47]

2.6 Survivability in RF field

The successful operation of a photocathode in accelerator RF injectors is determined by their survivability. Many photocathodes, metallic or semiconductor materials, were tested as electron sources in accelerator injectors. Bi-alkali photocathodes such as Cs_2Te and K_2CsSb survive several months in operation, independent on DC or RF injector.[48,49]

Contrary, the successful operation in SRF injectors is more challenging than in DC or RF injectors. The operation of photocathodes based on cesium (Cs) and its compounds is quite difficult compared to bulk metal cathodes. One of the most common challenges is the possible vaporization of cathode components into the cavity system, causing photocathode degradation. There is a strong need to maintain the cathode at a suitable temperature inside of the cryogenic SRF environment. For example, the overheated Cs_2Te in ELBE resulted in such a contamination of the cavity.[23,50]

Furthermore, the possibility of field emission at high fields and multi-pacting at low fields should be taken into account. It is important to note that a successful example for a long survivability of a bi-alkali (K_2CsSb) photocathode can be given.[51]

2.7 Electrical conductivity

The electrical conductivity plays a decisive role when dealing with photocathodes because electrons are permanently released from the material surface. As a logical consequence, the surface of the material remains ionized until the material can draw electrons *via* the contact to the cathode body and neutralize the caused ionization. If the photocathode is not able to track new electrons *via* the contact over the cathode body, the surface remains ionized. Thus, the photocathode is going to run out of its electrons and consequently, the cathode will lose QE.

Pure semiconductors are much less conducting than metals because the electrical conductivity of semiconductors depends on many factors such as temperature, pressure, and the concentration of supplied impurities.[5] Through the implantation of impurities, so called dopants, into the intrinsic semiconductor crystal lattice, the conductivity can be increased and varied. Dopant atoms replace the native host atoms in its intrinsic crystal lattice. Ideally, dopant atoms should have the same size as the host atoms, meaning the selection of a dopant nearby the position of the intrinsic semiconductor host atom in the periodic table of elements. The dopant atom has one greater or one fewer electron in the valence shell than the host atom.

3 Photoemission models: one step and three-step model

Two approaches are commonly used to describe the photoemission process, namely, the one-step model[52] and the three-step model, both summarized in Fig. 2.

The one-step model uses an approximation where electrons are excited from a bound state to a free state out of the material. The model assumes a well-defined crystalline state and is often used to study the band structure. For many photoemissive materials the one-step model is not practical as it does not take electron scattering effects into account.

The three-step photoemission model was developed by Berglund and Spicer[53] and is shown in Fig. 2 on the right side. As the name suggests, the photoemission process of this model is explained in three steps, consisting of the optical excitation, the transportation of the electron towards the surface and its

Open Access Article. Published on 17 2023. Downloaded on 05.11.2024 09:24:16.
This article is licensed under a Creative Commons Attribution-NonCommercial 3.0 Unported Licence.

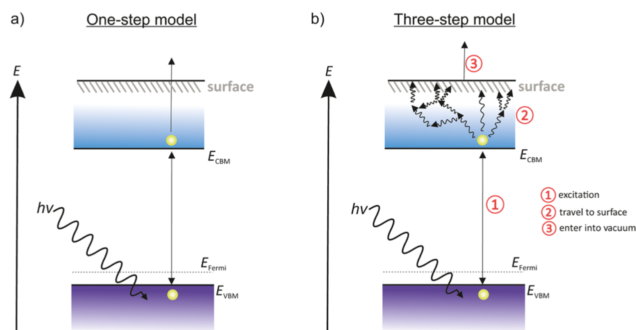

Fig. 2 Comparative illustration of (a) the one-step model and (b) the three-step model.

escape into the vacuum. The three steps are treated independently and separately from each other.

The first of three steps is the excitation from VB to CB. The electrons of the VB absorb the energy of the incident photons and are injected into the CB. This step happens only if the incident photons have enough energy to lift the electrons over the E_{gap} barrier.

The second step describes the scattering events. The photoelectrons in the CB move to the cathode surface *via* diffusion or drifting. During this process the electrons lose a part of their energy due to scattering or recombination with other atoms. This step enlarges the energy spread of photoelectrons.

The last step represents the release of the photoelectrons into the vacuum. The photoelectrons reach the surface and have to pass the E_{vac} barrier in order to escape into the vacuum. To make it easier for the photoelectrons, it is advantageous to reduce E_{vac} as much as possible, for example with the deposition of a thin film of a low work-function material, such as alkali–metals. As a consequence, the E_{vac} is close to the energy of the CB or situates below the CBM. This state is called a negative electron affinity (NEA) surface.

Considering metal photocathodes with no band structure, incident photons are absorbed and electrons are moving towards to the surface in order to escape into the vacuum. With a high probability of scattering events with other electrons, most of the traveling electrons lose nearly all of their energy in the way that they are no longer able to escape the cathode surface. Only electrons within one electron mean free path are able to escape the surface. Therefore, metal photocathodes have a generally low QE.

Semiconductors show a much higher QE compared to metal photocathodes. Incident photons with an energy higher than the E_{gap}, excite electrons from the VB into the CB. Once the photoelectrons enter the CB, almost no scattering from electron–electron collision can occur. Thus the electron mean free path of photoelectrons in semiconductors is much longer than in metals. Consequently, more photoelectrons are able to escape the surface and contribute to the QE. Scattering processes in grain boundary or lattice scattering still occur, but the photoelectrons loose only a small part of their energy.[5]

These two important and widely used models of the photoemission process can be further extended with the help of simulation methods such as Monte-Carlo,[54–57] density functional theory (DFT)[58–62] and machine learning.[63–68] DFT, for example, is used to calculate energy states based on electron densities and their energies. The calculations show different scenarios of covalent binding interactions between different atoms and the resulting work functions.[69] Thus, the formation of a dipole Ga–O–Cs layer in a Cs and oxygen (O_2) activated GaN and GaAs can be assumed.[23,51] The DFT calculations support experimental results well and can explain why the assumed formation of Ga–O–Cs on the surface plays an important role in achieving NEA surfaces. Due to this dipole layer sequence, researchers like Machuca[70] and Wu[71] tried to apply O_2 first in the preparation process. The goal was to form a more stable Ga–O_x foundation before Cs is applied to the semiconductor surface with the aim to achieve a higher QE.

4 Metal photocathodes

In the following sections the most common materials for photoinjectors are presented. The materials are described and summarized regarding their preparation method and their quality such as QE, lifetime, response time and thermal emittance. References are taken from international labs such as DESY, CERN, BNL, Jefferson Lab (JLAB), Italian Institute for Nuclear Physics (INFN), KEK and ELBE.

We compare metal photocathodes (section 4) possessing low QE with semiconductor photocathodes (section 5) possessing high QE.

Pure metal photocathodes such as Cu, Mg or Pb have a high work function and require ultra-violet (UV) light, which is the biggest disadvantage for high average current applications. However, metal photocathodes have also some advantages. The biggest advantage is their high robustness, so that they can survive years in operation.[33,50] Mg has a relatively low work function (3.6 eV) compared to Cu (4.6 eV) or Pb (4.3 eV). Mg can provide a QE of about 0.2% when illuminated with 258 nm UV light after a proper cleaning process.[29] Another advantage is that the preparation of such metal photocathodes is less complex compared to the preparation of semiconductor photocathodes, which is further described in the following sections.

4.1 Preparation

The most commonly used cleaning method is the thermal cleaning in vacuum environment. Once the cathode is installed in a UHV chamber, it undergoes a thermal cleaning at a certain temperature with the aim to desorb adsorbates such as water (H_2O), hydrogen (H_2), carbon monoxide (CO) and carbon dioxide (CO_2) from its surface. The typical thermal cleaning temperature can be varied between 200–300 °C and is applied for several hours or is even kept up to one day. Beside the thermal cleaning in vacuum, UV ozone (O_3) laser cleaning, hydrogen (H^+) or argon ion (Ar^+) sputter-cleaning should be considered as well.[39,50,72]

This journal is © The Royal Society of Chemistry 2023

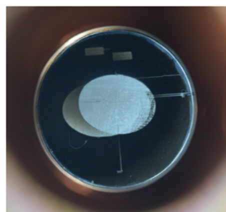

Fig. 3 Photograph of a 10 mm Mg cathode inside the UHV chamber. The middle bluish part of a spot size of 4 mm was cleaned with an UV laser.

An UV laser cleaning represents a suitable method and is used for the surface cleaning of a Mg cathode in ELBE. The Mg cathode consist of a 10 mm, high purity (99.999%) plug and undergoes an UV laser cleaning with 258 nm, 100 kHz repetition rate and 100 mW laser power. The area cleaned by UV light is seen as a 4 mm bluish spot in the middle of the 10 mm original Mg plug, shown in Fig. 3. This cleaning process is repeatable and thus the cathode can be reused several times.[29] Even when the cathode is exposed to poisonous gases, the UV laser cleaning can be used to remove adsorbed gases from the surface and to create a clean Mg surface once again.

Metal cathodes are mostly treated with a soft chemical cleaning and undergo a surface polishing till a polished mirror-like surface is achieved. The mirror-like metal cathode is stored under protection gas atmosphere until it is installed in the UHV chamber.

Other metal photocathodes such as Cu[73] or Pb,[74] used in BNL and DESY, are prepared in the same way as Mg cathodes.

4.2 Quantum efficiency and lifetime

Metal cathodes show relatively low QE values in the range of 10^{-4} to 10^{-1} compared to semiconductor photocathodes.[33] As mentioned in Section 3, this is caused by the energy loss due to scattering events and only electrons with one electron free mean path are able to enter into the vacuum.

It is well known that the photoemission process in metals takes place in the first surface layers[75,76] and therefore strongly depends on the surface quality. To be briefly exposed to air is less hazardous for metal photocathodes than for cesiated photocathodes.[29] Thus, the QE of the metal cathode drops less by a short exposure. Of course, the exposition to gases for longer time causes oxidation and leads to a change of the surface work function.

4.3 Thermal emittance

The thermal emittance is strongly influenced by the photocathode surface roughness and its morphology. The average roughness has to be as low as possible to reduce the probability of unwanted emittance. A commonly and widely used practice is the usage of a cathode with a diamond-turned surface, having an average roughness of less than 5 nm.[73] The values for the divergence of the electron beam, caused by the emission of metal cathodes are about 0.41 ± 0.03 mm mrad^{-1}.[77] For the thermal emittance of Mg photocathodes multiple publications showed a low value with an upper limit of 0.5 mm mrad mm^{-1}, driven with 4.66 eV in the warm RF gun.[78,79] Thus, Mg is a good candidate for high brightness photocathodes.

The application of an electric field can be beneficial to reduce the work function and consequently to increase the QE. This effect is called Schottky effect.[7] The original work function including the Schottky effect is combined into a new term, the effective work function.

Michaelson[80] showed that the work function not only depends on the surface quality and vacuum conditions, but also on the crystal orientation of the metal. Studies showed that the use of a single crystal benefits the photoemission to be more uniform compared to the photoemission of a polycrystal.[81] Since then studies were carried out how the crystal orientation and its roughness influences the beam parameters, *e.g.* the mean transverse energy spread.[82] However, it should be noted that inspite of the expected advantages of monocrystals, the polycrystalline cathodes are still widely used.[29,83]

The thermal emittance of a Cu photocathode was measured by H. Qian in a RF gun at 50 MV m^{-1} and showed 0.92 mm,[79] when it was illuminated with a 266 nm UV laser.

4.4 Response time

The response time for Cu and Mg cathodes is less than picoseconds.[7,84] Therefore, metal photocathodes are often used for accelerator applications where only low average current, and a fast response time is required.[5]

To sum up, metal cathodes should be considered as robust photocathodes for any type of injector, providing an average electron beam with acceptable QE.

5 Semiconductor photocathodes

Semiconductor photocathodes are sub-divided into positive electron affinity cathodes (PEA) and negative electron affinity cathodes (NEA). The main difference between the two types is the location of the E_{vac}, shown in Fig. 4. For PEA cathodes E_{vac} is above the CBM and for NEA cathodes E_{vac} is below the CBM.[25] Cs_2Te and alkali antimonide belong to PEA cathodes, whereas GaAs and GaN belong to NEA cathodes.

The semiconductor photocathodes for particle accelerators are further sub-divided according to their fabrication method:

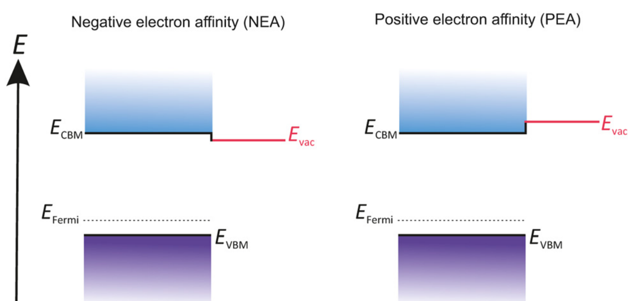

Fig. 4 Comparative illustration of the difference between PEA and NEA surfaces regarding the location of the E_{vac}.

Open Access Article. Published on 17 2023. Downloaded on 05.11.2024 09:24:16.
This article is licensed under a Creative Commons Attribution-NonCommercial 3.0 Unported Licence.

Open Access Article. Published on 17 2023. Downloaded on 05.11.2024 09:24:16.
This article is licensed under a Creative Commons Attribution-NonCommercial 3.0 Unported Licence.

(i) crystals grown on a substrate or (ii) the deposition of Cs and O_2 on an as-received semiconductor. Cs_2Te and antimonide photocathodes belong to (i) and are typically grown on a substrate that has to be cleaned in advance before the crystal growth can be realized.

In contrast semiconductors such as GaAs and GaN are commercially available and only a deposition of Cs and an electronegative ingredient such as O_2 are needed to obtain a photocathode. Therefore, these semiconductor photocathodes belong to (ii).

5.1 Cesium telluride

Alkali metals such as potassium (K), sodium (Na) and Cs have only one electron in the outer shell of their electron configuration. This single electron in the outer shell has a great affinity to form a new ionic bond with others. Tellurium (Te) has two single electrons in his 4p electron orbitals which react easily with alkali metals like Cs and form a stable compound material. One of the most used semiconductor compound materials as a photocathode in photoinjectors is Cs_2Te, which provides a long operational lifetime and a high QE.

5.1.1 Preparation. The standard growth process was established by Di Bona *et al.*[40] and the layer sequence of the prepared Cs_2Te is shown in Fig. 5.

The initial conditions for this type of photocathodes are UHV and highest purity of evaporators. In this established process, Cu or molybdenum (Mo) can be used as a substrate, which should be mirror-like polished and cleaned with acetone and ethanol in advance. The mirror-like polished substrate is then installed in the UHV chamber and heated up to 500 °C for 30 min. This thermal cleaning aims to remove residual adsorbates like gases or particles from the substrate surface. After the substrate is outgassed, it is kept at 120 °C. On this hot substrate Te and Cs are deposited in sequence, meaning at first Te and afterwards Cs. During the Cs deposition the cathode is illuminated with UV light to detect the photocurrent simultaneously. The photocurrent increased depending on the deposited amount of Cs on the Te layer. The Cs deposition is finished when the photocurrent exceeds a maximum and starts to descend.

Besides this sequential deposition process, a co-evaporation of Cs and Te at the same time is optional.[85] Both techniques deliver high quality and reproducible cathodes. The thickness is monitored by a quartz micro balance crystal during the manufacturing process.

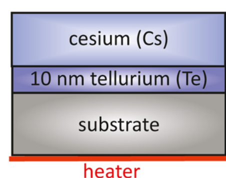

Fig. 5 Schematic overview of a typical layer sequence for a Cs_2Te photocathode, based on the original approach taken from ref. 40.

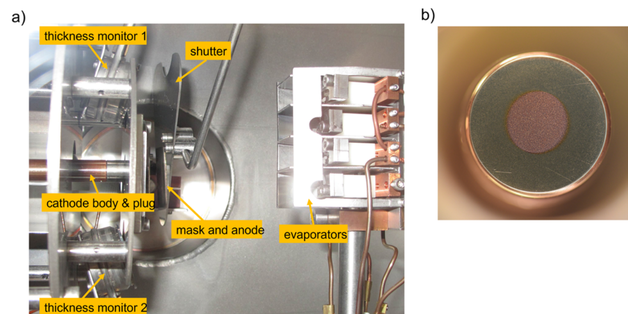

Fig. 6 (a) The interior of the Cs_2Te preparation chamber, showing a cathode body with a plug, shutter, a mask which is also an anode, two thickness monitors, and Cs and Te evaporators and (b) photo of a freshly deposited Cs_2Te layer (4 mm in diameter) on a Cu plug.

The substrate has an high influence on the performance of the grown Cs_2Te photocathode. It is well known that substrate atoms can diffuse into the deposited film or the substrate crystal structure does not match to the crystal structure of the photocathode. Thus, lattice mismatch happens. Furthermore, Cu atoms diffuse into Te and cause some island growth which leads to a lower QE compared to the Cs_2Te cathode on a Mo substrate.[40] Besides the standard substrates (Cu and Mo), Nb[86] can be considered as a potential substrate for Cs_2Te.

Fig. 6a shows an example of the main components of the preparation chamber at ELBE (left side), containing the Cs and Te evaporators from SAES and a mask between the cathode body and dispensers. The freshly prepared Cs_2Te photocathode can be seen in Fig. 6b on the right side. The grown Cs_2Te crystal is 4.0 mm in diameter on a Cu substrate and has a violet color, which appears orange due to light incidence in Fig. 6b.

5.1.2 Quantum efficiency. The QE is influenced by many factors such as the quality of the evaporators, the thickness of the deposited layer and the residual gas impurities in the UHV chamber. At INFN, Cs_2Te showed QE values of 10% or more,[87] in which Cs_2Te was grown by a sequential deposition. Afterwards the Cs_2Te was stored in an UHV transport chamber and was send to DESY. During the transportation the photocathode did not lose QE significantly.[88–90]

Especially the thickness of the deposited Cs_2Te layer plays a superior role in the QE performance and is still under optimization at DESY and INFN.[91,92]

High QE of Cs_2Te can be achieved only under an UV-excitation, which is the biggest disadvantage of this photocathode compared to the antimonide-based photocathodes that are operating under green light, as described in the next chapter. Another disadvantage is the high sensitivity to any residual CO_2 or O_2 molecules in the UHV system. The adsorption of gas molecules changes the surface work function negatively so that the QE drops. Further detailed information is given in Section 5.1.4.

5.1.3 Thermal emittance. As mentioned in Section 4.3, the thermal emittance is strongly influenced by many parameters such as cathode surface, applied electric field, laser spot size

 This journal is © The Royal Society of Chemistry 2023

Open Access Article. Published on 17 2023. Downloaded on 05.11.2024 09:24:16.
This article is licensed under a Creative Commons Attribution-NonCommercial 3.0 Unported Licence.

and incident wavelength. Typical values for Cs_2Te photocathodes are between 0.6–1.14 μm mm^{-1}.[93,94]

Cs_2Te has a MTE of 0.55 eV and a thermal emittance of 0.43 π mm mrad mm^{-1} from Floettmanns estimation.[95] In ELBE SRF gun, the thermal emittance of an old Cs_2Te cathode (QE was below 1% at 258 nm) was measured 0.6–0.7 mrad mm^{-1}, and the average kinetic energy was about 0.35 eV.[96] However, the thermal emittance of Cs_2Te was measured by P. Huang and reached about 1.1 π mm mrad mm^{-1} in the warm RF gun at 40 MV m^{-1} and at 257 nm of the drive laser.[97]

5.1.4 Lifetime. The vacuum conditions have a high impact on the lifetime of the cathodes.[98] Chanlek *et al.* studied the lifetime and surface composition of Cs_2Te cathodes under exposure to different gases such as O_2, CO_2, CO, nitrogen (N_2) and methane (CH_4).[99] The QE decayed exponentially depending on the amount of O_2 and CO_2, measured by the partial pressure in the UHV chamber. The studies showed that O_2 and CO_2 were toxic for the Cs_2Te cathode. However, the poisoned cathode can be rejuvenated, if it was treated with 254 nm UV-light at 230 °C for one hour.

In its own turn, CO, N_2 and CH_4 did not show any significant effect on the lifetime of the Cs_2Te cathodes.[40]

5.1.5 Response time. The direct measurement of the response time of 350 fs in an RF injector was reported at KEK.[46] Furthermore, response times under RF conditions related to different Cs_2Te layer thicknesses were investigated at DESY.[92] The study compared Cs_2Te cathodes with different film thicknesses produced at INFN and homemade 100 mm Cs_2Te cathodes produced at DESY. All Cs_2Te photocathodes showed prompt response times in 180–250 fs range.[100] Cs_2Te provides therefore a prompt response time, which is beneficial for ultra short pulse generation.

5.1.6 Survivability in RF field. An advantage of Cs_2Te is its robustness under RF fields.[101] Thus, it can be used in RF and in SRF injector systems for a long time.[90,102] If no vacuum instability occurs and thus the Cs_2Te layer is not influenced negatively, it can be operated several months or even for over one year.

Summarizing, Cs_2Te is a good choice as it shows a reasonable QE, lifetime, fast response time and a good survivability under RF fields. The preparation is relatively simple and guarantees QE values between 10–20% under UV excitation. The main disadvantage, besides the requirement of intensive UV light, is its low robustness against vacuum instabilities, especially against O_2 and CO_2. The rejuvenation of the poisoned cathode is possible, but requires UV light and additional thermal treatment.

5.2 Alkali–metal antimonide

This family of alkali–metal-antimonide photocathodes includes a large variety of different compositions of alkali metals combined with antimony (Sb). Commonly used photocathodes are Cs_3Sb, K_2CsSb, Na_2 KSb and Na_2 KSb(Cs). They are widely applied in particle accelerator systems. In the following we focus only on the potassium cesium antimonide (K_2CsSb) cathode as the most representative member of this family.

5.2.1 Preparation. Sommer *et al.* reported a new photoemissive material using Sb combined with alkali metals in 1955.[103] The original recipe describes the deposition of 10 nm Sb, followed by 20 nm of K and Cs until a maximum photocurrent is reached. The original layer sequence is shown in Fig. 7. The production of antimonide cathodes can be performed as sequential or co-evaporation, similar to the preparation of Cs_2Te cathodes. As usual for all photocathodes, it is necessary to work in a UHV chamber to guarantee a high quality of the photocathode crystal without unwanted impurities. Ongoing study and optimization of the antimonide cathode preparation is still in progress aiming to improve the preparation recipe and the QE.

Any adsorption of gases like H_2, O_2, CO, CO_2 or H_2O will poison the photoemissive layer and disturb the crystal lattice, leading to a reduced QE.[104]

The key parameter of this type of cathode was the K layer thickness that was studied by BNL.[51] The highest QE was achieved with a Sb : K ratio of 1 : 2.2, which means 10 nm Sb and about 22 nm K was deposited. A longer deposition of K would lead to the formation of tri-potassium antimony (K_3Sb) that prevents the subsequent diffusion of deposited Cs.

The freshly prepared cathode could be transported in a UHV suitcase into the SRF Gun. During the transportation the cathode lost some QE that was caused by vacuum instabilities. Despite of this loss, the remained QE was still sufficient enough for the applications in SRF guns. Seen as a suggestion, a preparation next to the injector reduces the transportation difficulties and can be beneficial for the QE of the photocathode.

5.2.2 Quantum efficiency. K_2CsSb photocathodes provide a QE between 4–12% at 532 nm and low thermal emittance.[51,104,105] The main advantage of the K_2CsSb cathode is its spectral response under green light. Therefore, it is also called "green cathode". Compared to other cathode materials operating under UV-light, this green cathode type relieves the laser system because only the second harmonic transformation of the laser is needed.

5.2.3 Thermal emittance. A thermal emittance value for a K_2CsSb photocathode was published at 0.56 ± 0.03 mm mrad mm^{-1} at 532 nm and the MTE was 160 ± 10 meV.[106] This study also showed that for the relating antimonide photocathodes (Cs_3Sb) the same value can be achieved.[47] One should consider that the thermal emittance for this type of photocathode is lower than for Cs_2Te photocathodes. In other publications K_2CsSb

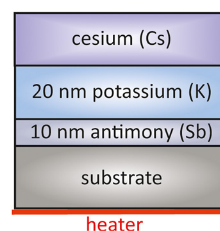

Fig. 7 Schematic overview of a typical layer sequence for a K_2CsSb photocathode, based on the original approach taken from ref. 51.

Open Access Article. Published on 17 2023. Downloaded on 05.11.2024 09:24:16.
This article is licensed under a Creative Commons Attribution-NonCommercial 3.0 Unported Licence.

photocathodes were studied with an electric field at the photocathode of 2.2 MV m^{-1} and driven by a 533 nm laser in JLab DC photojector. The thermal emittance was reported with 0.4 mm mrad mm^{-1} per rms laser spot size.[107]

5.2.4 Lifetime. Wang *et al.* investigated in the occurrence of multi-pacting and its influence on the quality of different antimonide cathodes operating in the SRF Gun.[51] Multi-pacting is a common phenomenon of the resonant electron discharge, which occurs under RF fields. The emitted electrons lead to exponential electron multiplication in the alternating RF electric field when certain conditions are satisfied. This unwanted electron avalanche is defined as multi-pacting and is located mostly in the gap between cathode and RF device or on dielectric surfaces. It can cause significant damage to RF devices.

The main difference between the cathodes from Wang *et al.* was the diameter size of the deposited bi-alkalides on the substrate surface. The cathode where the entire 20 mm substrate surface was covered by K_2CsSb showed high multi-pacting and degraded fast, which meant a fast exponential decay in the QE. Additionally, a degradation in the SRF gun performance was also recognized, which was related to the release of photocathode incidences into the cavity downstream. Nevertheless, the group showed that the cathodes survived at least 20 days in the SRF gun.[51]

5.2.5 Survivability in RF Field. K_2CsSb photocathodes are widely applied in DC gun injectors.[106] The first successful operation of a K_2CsSb photocathode in an RF injector was reported by Dowell in 1993,[105] while the first successful application in SRF injectors was demonstrated in 2018.[51,104] The cathode has to face more difficulties in SRF Guns than in DC injectors. A big problem in RF injectors is the potential risk of multi-pacting. However, as it was mentioned above, Wang *et al.* recently reported about the successful operation of a bi-alkali photocathode up to nearly one month in an SRF Gun.[51]

Summarizing, K_2CsSb cathodes have many advantages due to their high QE and low thermal emittance. Nevertheless, the difficulties related to the complex preparation with the precise ratio of an optimal composition in order to gain a high QE and a long lifetime should be taken into account. One should also consider the limited lifetime under RF fields and the potential risk of cavity contamination, when used in (S)RF injectors.

5.3 Gallium arsenide

In contrast to Cs_2Te and K_2CsSb photocathodes, GaAs and GaN semiconductors are already grown on a substrate. Both semiconductors are commercially available with reproducible quality which is a benefit as the desired quality and the dopant concentrations can be guaranteed by the supplier.

GaAs is a semiconductor with a zinc blende structure and a direct band gap, which makes the photo-excitation energetically more favorable as in case of indirect band gap semiconductors. For the photoemission, p-doping is needed, which means that one lattice site of the original host atom is replaced to an atom with one valence electron less. This causes the appearance of holes in the lattice structure. Another benefit of

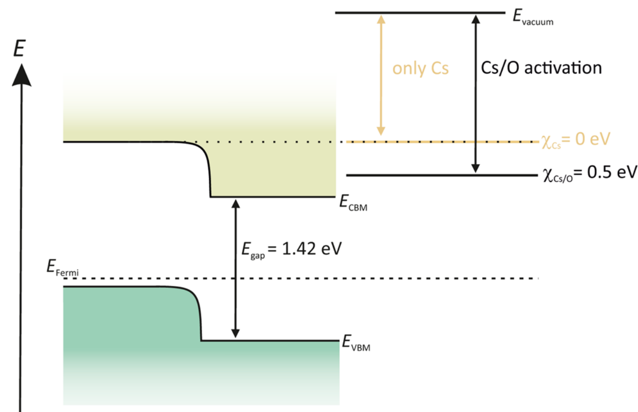

Fig. 8 Schematic drawing of the band structure of p-GaAs, activated in a YoYo process with Cs and O_2.

the p-doping is its responsibility to introduce band bending, shown in Fig. 8. The p-doping lowers the CB, thus reducing the EA energy. With the deposition of Cs on the surface, the E_{vac} can be lowered to the same energy level as the CB. Therefore it is not possible for photoelectrons to enter into the vacuum. By adding a strong electronegative oxidant such as O_2 or nitrogen tri-fluoride (NF_3) the E_{vac} can be further reduced below the CBM and photoelectrons will now be able to leave the GaAs surface (Fig. 8).[108,109]

Since Scheer and Laar proposed GaAs as a photoemitter,[110] this material found broad applications in photodetectors,[111] electron microscopes[112] and photon-enhanced thermionic emission devices.[113] Its good spectral response to near infrared (NIR) and low dark current makes it suitable to vacuum photodetectors. The possibility to reach a high current density under excitation by visible lasers, spin-polarization, low thermal emittance and a narrow energy distribution fit to the requirements of high brightness electron sources for FEL, energy recovery lines (ERL) and THz devices.[114] GaAs absorbs a broad wavelength spectrum and has the ability to emit spin-polarized photoelectrons when illuminated with polarized NIR light.[108] The emission of spin-polarized electrons represents the main advantage and plays an increasing role in high energy physics. The spin-polarized electrons are used in combination with accelerator technology in transmission electron microscopy when using GaAs superlattices in order to create magnetic field images with high resolutions.[5]

A faster response time and a high spin-polarization electron yield was recently achieved by a gallium arsenide phosphide (GaAsP) superlattice photocathode.[115] The rapid development in the research on GaAs/GaAsP superlattice photocathodes offers new research fields for more advanced semiconductor photocathodes and their potential application as an electron source.

5.3.1 Preparation. A surface cleaning prior to the activation with Cs and O_2 is required for commercially available GaAs. The wet chemical cleaning differs from lab to lab and some labs prefer just a simple solvent cleaning in acetone or ethanol, while other labs apply an etching in hydrochloric acid (HCl)

 This journal is © The Royal Society of Chemistry 2023

Open Access Article. Published on 17 2023. Downloaded on 05.11.2024 09:24:16.
This article is licensed under a Creative Commons Attribution-NonCommercial 3.0 Unported Licence.

solutions or a mixture of highly diluted sulfuric acid and hydrogen peroxide (H_2SO_4/H_2O_2).[116–119]

An alternative to wet chemical cleaning represents ion-sputtering that allows to achieve an atomically clean surface.[120] This technique uses energetic ions, such as argon (Ar^+) or hydrogen (H^+), bombarding the semiconductor surface in order to remove surface adsorbates. The disadvantage of ion sputtering lies in the potential risk of surface damage, decomposition and higher surface roughness.[121]

However, the more usual way is to thermally clean the GaAs surface at 500–600 °C for minimum half an hour in UHV environment. As already mentioned before, the aim of the thermal cleaning is to obtain a chemically clean and uniform GaAs surface, which can be examined by *ex situ* or *in situ* surface studies, such as X-ray photoelectron spectroscopy (XPS).

Togawa *et al.* showed that GaAs was activated in a so-called YoYo process, after it has been thermally cleaned.[122] The YoYo process consisted of the sequential deposition of Cs and O_2 to receive a NEA surface, shown in Fig. 9. The deposition process was monitored by a *in situ* photocurrent measurement. At first Cs was deposited excessively which was recognized by the descending photocurrent. Afterwards O_2 was added to the excessively cesiated surface. When the photocurrent reached a maximum and started to drop again, the deposition of O_2 was stopped. Each step of Cs and O_2 deposition was repeated several times until a final photocurrent was achieved. Other oxidative gases such as NF_3 could also be considered as a successful activation ingredient besides O_2.[123]

There is no clear recipe for the GaAs preparation as different facilities follow different activation conditions. Some researchers prefer to deposit Cs all the time and just turn on O_2 occasionally to increase the photocurrent when it is needed.[69] Therefore this method represents more a co-deposition, rather than a sequential deposition.

Recent investigations dealed with the theory of a dipole model of Ga–O–Cs and its relevance to form a NEA surface.[124–126] Furthermore, the importance of a clean GaAs surface was discussed in 2020.[119] Since photocathode research started, it was well known that the surface cleanness has a great influence on the photoemission performance. As mentioned in the sections above, the surface can be contaminated easily with various organic substances, oxides and air components. Therefore, Zhang *et al.* studied the p-GaAs performance depending on different cleaning processes.[127] The surface composition and its potential contaminations hindered the Cs/O_2 deposition to form a NEA surface. Therefore, it was impossible to form a proper Ga–O–Cs dipole layer if contaminants remained on the surface. Consequently, the photoemission performance was less than expected.

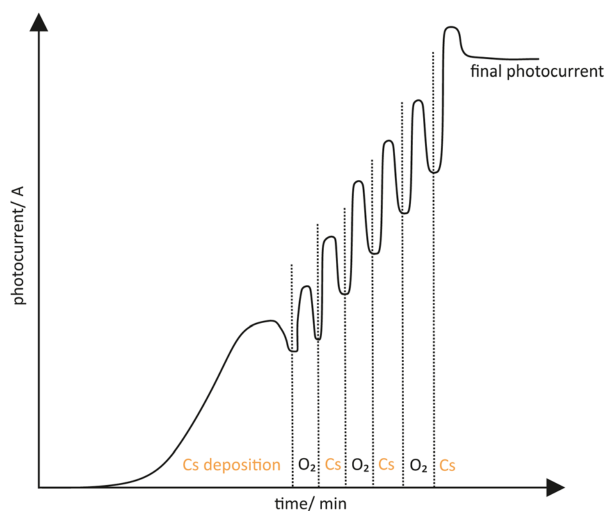

Fig. 9 Schematic drawing of a typical photocurrent evolution when a YoYo activation is used (alternately applying Cs and O_2).

5.3.2 Quantum efficiency. GaAs photocathodes provide a high QE (over 10%) in visible light and are often used to produce spin-polarized electron beams when illuminated with NIR light.[128] The main advantage of this material is that it does not require UV light to produce spin-polarized electrons. Thus, using visible light or NIR is a great relief of the laser instrumentation. Moreover, the application of GaAs layered structures and superlattices lead to higher polarization values but result in less QE.[129]

The QE of GaAs is affected by many other factors than those discussed in the sections above. Beside vacuum, material quality, incident wavelength, cathode temperature, Schottky effect and surface contaminations, the thickness of the GaAs layer, dopant concentration and NEA conditions play an immense role for the successful operation of this material. Therefore, the optimization of this material is still a hot topic in modern research.

5.3.3 Thermal emittance and response time. Thermal emittance and response time measurements of GaAs were investigated at CLASSE,[30] where measurements showed a prompt response time. At the same time, values for the thermal emittance for GaAs were found between 0.1–0.4 μm.[37,130] The thermal emittance could be lowered by using GaAsP superlattices and showed faster response times then for usual GaAs photocathodes.[115]

However, it should be pointed out that GaAs photocathodes show the lowest thermal emittance value compared to other known photocathodes. Regarding to the thermal emittance, our analysis of the literature data shows that further research on these issues is strongly demanded.

One problem of GaAs photocathodes is the variation of the response time with the wavelength of the incident light. The penetration depth of the incident light depends on its wavelength. Near the band gap photoelectrons are generated deep in the material. The deeper the photoelectrons are generated in the material, the longer they need to travel towards to the surface. In fact this means that a longer extraction time gives them more time to thermalize and therefore they do not contribute anymore to the QE. Therefore, a thin layer of GaAs on a glass substrate, operating in transmission mode, is used to overcome this problem.[131]

5.3.4 Lifetime. Reaching a long lifetime of GaAs photocathodes is still a challenging task because this type of

Open Access Article. Published on 17 2023. Downloaded on 05.11.2024 09:24:16.
This article is licensed under a Creative Commons Attribution-NonCommercial 3.0 Unported Licence.

photocathode shows a fast degradation due to its sensitivity to any residual gases.[41] Therefore, it requires ultimate UHV conditions. The main reasons for its fast degradation are ion back-bombardment, high-voltage application and destructive heat load under intensive illumination. Ion back bombardment and sub-optimal vacuum conditions influence the surface composition negatively, resulting in a poisoned surface that prevents the desired photoemission.[99] The lifetime can be improved if the activation process is optimized. Possible solutions include the application of different novel oxidants as well as elucidation of the role of N_2.[123,126]

In the last years, research was carried out to protect the GaAs emission layer with a Cs_2Te[116,129] or a Cs–Sb protection layer.[132] The Cs_2Te protection layer was able to extend the lifetime of GaAs significantly, resulting in a five times slower QE decay than for GaAs photocathodes without such a protection layer.[133]

5.3.5 Survivability in RF Field. GaAs is already successfully applied in DC Guns[126] and its potential application in RF injectors is still in test phase.[134] Furthermore, GaAs could be operated in two different ways as shown in Fig. 10. GaAs can be used in transmission or in reflective mode, which depends on the direction of the incident light. In transmission mode the photocathode is illuminated from the backside through the substrate material. The requirements for the substrate are to be transparent for the wavelength of interest.

Contrary, in the reflective mode the photocathode is illuminated from the frontside with the incident light. Both techniques are illustrated in Fig. 10 where photoelectrons are generated and travel in all directions through the GaAs layer.

5.3.6 Spin-polarization. As already mentioned, GaAs has the ability to produce spin-polarized electrons. The nature of this polarization lays in the spin–orbit splitting of the valence band. The valence p band is splitted into fourfold $p_{3/2}$ levels and twofold $p_{1/2}$ levels, shown in Fig. 11.

The energy difference of these levels is 0.34 eV and the electron transition rule is $\Delta m = \pm 1$. This means m is for positive

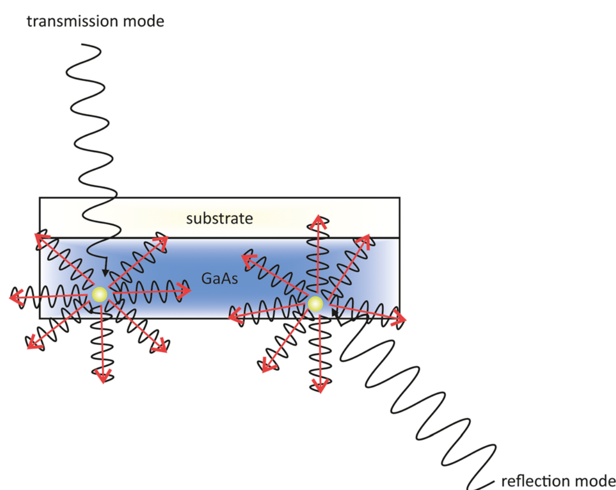

Fig. 10 Schematic drawing of the difference in the incident light paths in a transmission (left) and reflection mode (right) GaAs photocathode.

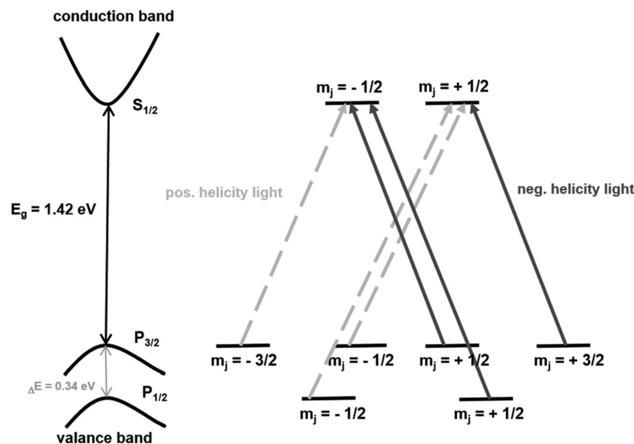

Fig. 11 Schematic representation of the electron transitions for the generation of spin-polarized electrons in GaAs photocathodes.

helicity light +1 and for negative helicity light −1. Some transitions are more favourable than others and thus the probability for positive helicity light is three times higher as more electrons are lifted into the $m = -1/2$ state than into the $m = +1/2$ state.[135] When electrons are excited from the spin–orbit-splitt-off band, no polarization occurs at all. In contrast, a maximum polarization is obtained for a photon energy exceeding the band gap energy for less than 0.1 eV. A big advantage is the easily achievable polarization reversibility as the incident irradiation can be changed externally.

The main drawback of GaAs for high polarization is its reduced QE. Usually the electron spin-polarization yield (ESP) is between 30–50%, depending on dopant concentration, temperature and the operation mode for unstrained bulk GaAs.[136,137] Demonstrations at SLAC showed that a polarization yield up to 80% was achieved with high-gradient doped strained GaAs.[138] However, the highest polarization yield of 84% at 6.4% QE was reported on superlattice structured GaAs with a distributed Bragg reflector (DBR).[139]

To sum up, GaAs is the only photocathode at the moment which is able to produce spin-polarized electrons. Its spectral response in NIR is advantageous because no UV laser is needed. On the other side GaAs as a photocathode has many disadvantages such as the complex activation with alternatively Cs and O_2. One should also consider the very strict requirement on stable UHV vacuum conditions. The limited lifetime and the risk of multi-pacting and its consequences are very high when the photocathode is used in a RF field. Thus, more studies regarding this issue are necessary.

5.4 Gallium nitride

III-Nitride semiconductors are widely used for blue, green and UV light-emitting diodes.[140] The adsorption range in UV- and visible light characterizes these compound materials as potential photocathodes. GaN as a photocathode is expected to be robuster and can achieve a higher QE than other photocathodes.[141] The potential application in particle accelerator injectors is quite new and up to now not tested.

 This journal is © The Royal Society of Chemistry 2023

Open Access Article. Published on 17 2023. Downloaded on 05.11.2024 09:24:16.
This article is licensed under a Creative Commons Attribution-NonCommercial 3.0 Unported Licence.

The rapid development in semiconductor industry offer improved growth methods and new possibilities to manufacture structured photocathodes. The variation of the dopant concentration inside the emission layer in combination with different layer thicknesses have a high impact on the performance of the semiconductor photocathodes. This multivariability of the growth and doping methods makes a reliable comparison of photocathodes prepared by different groups at different facilities very difficult.

As a rule, usually Mg-doping is used to create a p-type GaN semiconductor and an optimal hole concentration of 10^{17} cm^{-3} is desired to achieve high QE.[142] Some publications refer to the Mg concentration instead of the hole concentration, whereby the hole concentration is estimated to be two orders of magnitude lower than the introduced Mg concentration.[143]

5.4.1 Quantum efficiency. Machuca *et al.* reported about a Cs-activated GaN that was robuster than other photocathodes and showed a QE of 53%.[141] A lower susceptibility to O_2 was discovered in this study when the Cs-activated GaN photocathode was exposed to O_2. Therefore, it showed a higher lifetime than GaAs photocathodes.

The highest QE for GaN-based photocathodes was reported by Uchiyama *et al.* where about 70% QE could be achieved depending on the p-dopant concentration.[143] This result showed that an optimal Mg dopant concentration was strongly required because it was beneficial for the photoelectrons to travel towards the surface.

The uniform-doping is widely applied in semiconductors, however, the photocathode performance can be increased with gradient-,[144] exponential-[145] and delta-doping[146,147] profiles. This possibility pushes the rapid development of advanced efficient GaN photocathodes because two times higher QE was achieved with gradient-doped GaN than with uniform-doping.[144]

Another important variable that has to be considered is the thickness of the buffer and emission layer. Nitride semiconductors are usually produced by metal–organic chemical vapor deposition (MOCVD), molecular beam epitaxy (MBE) or other physical deposition processes like magnetron sputtering (MSE).[140] Usually, a single crystal or hetero-epitaxial thin film is grown on a substrate such as silicon (Si), sapphire (Al_2O_3), silicon carbide (SiC) or spinel ($MgAl_2O_4$). The most commonly used substrate is Al_2O_3 because of its availability and low cost. Unfortunately, Al_2O_3 is not the substrate of choice because of the high lattice mismatch between Al_2O_3 and GaN of 16–17%, whereas GaN on SiC has only a lattice mismatch of 3%.[148,149] A high crystal quality with low lattice mismatch is necessary to guarantee a photocathode with high QE. Therefore often buffer layers (aluminum nitride (AlN), $Ga_{1-x}Al_xN$ or undoped GaN) of different thicknesses were grown on the substrate to reduce the lattice mismatch.

Additionally, the emission layer thickness plays an important role to achieve higher QE with nanostructured photocathodes. An optimal thickness guarantees the full absorption of the incident light without losing photoelectrons on their way to the surface. Different layer thicknesses were compared in transmission and reflection mode photocathodes.[150,151] The optimal emission layer thickness was found between 90–200 nm.[142] p-GaN nanowire photocathodes show higher QE than planar p-GaN photocathodes.[152] Xia *et al.* showed that the QE can be even further increased by using exponentially doped GaN nanowires.[153]

In the last years, graphene was found to be a potential new substrate for bi-alkali photocathodes.[154] The graphene substrate could be reused after an annealing at 500 °C and the renewed bi-alkali photocathode achieved similar QE values in the renewed process. Yayama *et al.* grew 2D GaN on a thin graphene sheet, supported by bulk GaN.[155] The suggested growth method leads to 2D GaN possessing novel advanced electronic properties. The introduction of a thin graphene sheet could also reduce the high lattice mismatch between GaN and other substrates, such as the widely used Al_2O_3 or Si. The cut-off spectral response for p-GaN photocathodes is usually at 360 nm[156] and thus a little relief of the UV-laser system can be guaranteed. However, the spectral response is adjustable by the manipulation of the E_{gap} with suitable dopant atoms. These dopants, such as indium (In) or phosphorous (P) can decrease the E_{gap} to a more suitable wavelength in the visible spectral range and recently published studies reported on the potential usage of such novel InGaN photocathodes.[157–159]

5.4.2 Preparation. The commercially available semiconductor undergoes a wet-chemical cleaning before being installed in a UHV chamber. A thermal cleaning at 500–750 °C for minimum half an hour is required prior to the activation. The thermal cleaning is aimed to obtain an atomically clean and uniform surface.[160] Smith *et al.* reported that a solely wet chemical treatment was not enough to remove carbon and O_2 contamination. Therefore, these authors investigated an additional thermal cleaning at 800 °C, where a decomposition of the semiconductor material occured.[161]

An activation with a thin alkali metal layer like Cs reduces the surface work function of GaN to form a NEA surface. As a consequence, the E_{vac} is shifted below the CBM energy level. Electrons excite over the E_{gap} and can easily enter into the vacuum, shown in Fig. 12.

Many studies were carried out recently dealing with the photoemission of GaN and the role of O_2 in its activation process.[109,162] It is widely accepted that the activation of GaN and GaAs photocathodes are different. Wang *et al.* reported that an activation of GaN with sequential Cs/O_2 gave no significant improvement compared to an activation with only Cs. When using Cs excessively, like in the YoYo process, it was assumed that more than a monolayer of Cs deposits onto the GaN surface. Consequently, the photocurrent decreased. If afterwards O_2 was introduced to the Cs-poisoned GaN surface, the photocurrent increased again, and the alternating cycle can be repeated until the photocurrent reached a maximum value.

The reason why O_2 is assumed to be not beneficial for GaN photocathodes, lays in the EA potential. When introducing Cs to the GaN surface, E_{vac} is reduced down to 3 eV. The new position of the E_{vac} is then already below the CBM. The E_{vac} can be only further 0.2 eV reduced when O_2 is introduced.

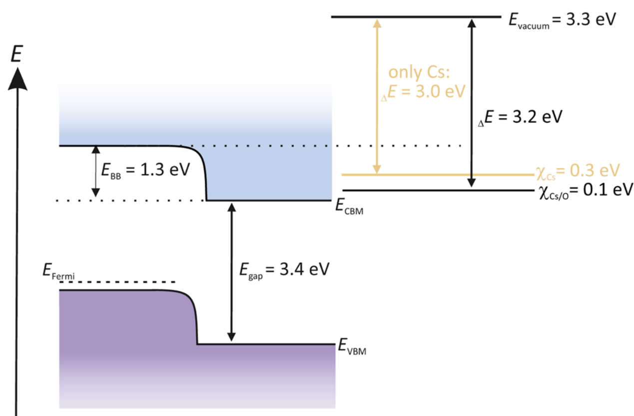

Fig. 12 Schematic representation of the band structure of p-GaN when activated with Cs and O_2.

Therefore, O_2 has no obvious benefit and thus is not necessary to obtain a NEA surface for GaN semiconductors.[163] In fact, this means that the activation for GaN with only Cs is more practicable and easier, compared to other photocathodes, such as GaAs or Cs_2Te.

5.4.3 Lifetime. The degradation of GaN photocathodes depending on the adsorption of O_2, CO and CO_2 was studied by Chanlek *et al.*[99] and represented a fundamental starting point for further GaN photocathode research. Iijima *et al.* reported on optimal temperatures between 150–300 °C that led to the desorption of surface molecules such as CO and CO_2.[41] This study also showed that a poisoned GaN surface was rejuvenated by a simple thermal treatment.

Amano *et al.* studied the QE recovery of Cs/O_2 activated p-GaN on Al_2O_3 and as-received n-GaAs by a thermal cleaning.[125] GaN was thermally cleaned at 500 °C and 600 °C and activated by a sequential Cs/O_2 deposition of a YoYo process. In this research the fresh photocathode was exposed to N_2, which lowered the QE three orders of magnitude. 60% of the initial QE was recovered with a new subsequential thermal cleaning. Thus, it is obvious that the re-activation of NEA cathodes is possible, but further studies are strongly recommended.

5.4.4 Thermal emittance and response time. Thermal emittance and response measurements for GaN photocathodes were studied at CLASSE.[30] The GaN photocathode showed a value of 1.35–0.11 mm mrad,[30] which is higher than for GaAs photocathodes. However, our analysis of the literature data shows that further research on these issues is strongly demanded.

5.4.5 Survivability in (S)RF Field. A lot of studies were carried out on GaN grown on Al_2O_3 because Al_2O_3 is a low cost and widely available substrate. However, insulator substrates are difficult to handle in injectors and thus, the photocathode potentially warms up under laser illumination and might be destroyed. Moreover, a potential release of Cs into the cavity can not be excluded as a result of thermalization.

An efficient and permanent heat dissipation is necessary to keep the cathode at convenient temperatures. To bypass the thermal conductivity problem of the substrate, Schumacher *et al.* investigated the deposition of p-GaN on Cu using a sputter magnetron method.[164] Cu provides a good thermal conductivity and should be considered as a potential substrate for GaN. To overcome the high lattice mismatch between GaN and Cu, an AlN buffer layer was introduced.

Summarizing, GaN shows an enormous potential as a future novel electron source in particle accelerators. Although p-GaN requires UV light like many other photocathodes, its spectral response is adjustable by the manipulation of the E_{gap} with suitable dopant atoms. Furthermore, p-GaN can be easier prepared as compared to other semiconductor cathodes, and it is possible to simplify its activation by applying exclusively Cs. A big advantage is the possibility to juvenile this cathode with a subsequent thermal treatment to remove the adsorbed pollutants from the surface when the photocathode degraded.

In the last year, a new idea of using non-activated GaN for spin-polarized electrons showed up.[165] The reason why GaN has the ability to produce spin-polarized electrons lies in its wurtzite crystal structure. The ongoing research has the aim to detach the highly sensitive GaAs-based photocathodes.

Furthermore, a more detailed information about GaN-based photocathodes can be found in a recently published review.[142]

6 Other photocathode ideas

A new idea is to use photocathodes with nano diamond layers, which can guarantee a higher QE than metal photocathodes.[166] The production with a pulsed spray technique is easier and has more advantages compared to CVD methods that need a hot substrate. With this new technique the nano diamond layers are deposited directly from a dispersion solution at low temperatures onto a substrate.

Another novel idea is the usage of titanium nitride (TiN) photocathodes, which seem to be promising for photoinjectors because they provided a prompt response time and a low thermal emittance as shown by An *et al.*[167] Unfortunately, the TiN photocathodes showed a low QE, which was assumed to derive from an O_2 or other surface contamination. By creating an atomically clean surface or by using a nanostructured TiN photocathode the QE could be potentially increased.

7 Conclusion and outlook

This paper summarizes the development of the existing photocathodes that are mostly used in particle accelerator photoinjectors.

Metal photocathodes such as Mg, Cu and Pb are simple in their surface cleaning which makes them easy to handle. Their biggest advantage is their high robustness against vacuum instabilities compared to semiconductor photocathodes. Even in case of surface oxidation, they can be rejuvenated after another surface cleaning. Their high work function makes them less efficient, and the strong desire of higher beam current leads to the usage of semiconductor photocathodes.

Open Access Article. Published on 17 2023. Downloaded on 05.11.2024 09:24:16.
This article is licensed under a Creative Commons Attribution-NonCommercial 3.0 Unported Licence.

Open Access Article. Published on 17 2023. Downloaded on 05.11.2024 09:24:16.
This article is licensed under a Creative Commons Attribution-NonCommercial 3.0 Unported Licence.

However, a robust metal cathode is the first choice for the commissioning of an photoinjector.

Besides metal cathodes, semiconductors such as Cs_2Te and K_2CsSb are the most commonly used photocathodes in particle accelerators. They provide high QE of above 10%, which makes them highly attractive. However, they are very sensitive to any vacuum instabilities and represent a risk for a potential contamination in the photoinjector due to the release of compound atoms. Moreover, the preparation of semiconductor photocathodes, consisting of a deposition of different compound materials on a substrate is more complicated than the simple cleaning of metal cathodes. One should take into account that even under the same conditions in the same laboratory the cathode quality can vary, depending on the quality of the semiconductor produced.

A special type of semiconductor photocathodes represent the III–V semiconductors, such as GaAs and GaN. These semiconductors are already grown on a substrate and commercially available. In order to produce a photocathode only a thin film deposition of Cs (and O_2) is needed.

GaAs is the cathode of choice if a spin-polarized beam or a low thermal emittance is desired. The preparation of the GaAs photocathode requires an alternate application of Cs and an electronegative component like O_2. The QE of GaAs resembles to those of other semiconductors, depending on the incident wavelength. A compromise between a high QE and a polarization rate has to be found because only one can be high while the other is low. The disadvantage of this cathode type is its short lifetime of approximately one hundred hours and also its potential release of Cs or other compounds into the injector system. Thus, the research for improving the lifetime of a GaAs photocathode is still ongoing.

Similar to GaAs, p-GaN can form a NEA surface to obtain a photocathode. A reported QE in the range of 40–70% is a good foundation for further research of this novel type of photocathode. None of the used cathodes in particle accelerators can provide such high QE values so far. Although p-GaN requires UV light, it guarantees a more stable NEA layer with less stringent vacuum conditions. With the possibility of modulating the E_{gap} by dopants such as In or P the requirements of the laser system could be relieved. Therefore, p-GaN photocathodes with a robust NEA layer show a high potential for high current applications. However, not all necessary parameters have been studied so far. Actual data about thermal emittance and response time are missing or need to be updated.

Further investigations have to be carried out on p-GaN photocathodes with the possibility of using much higher crystal quality and an optimal doping rate in p-GaN layers nowadays.

p-GaN and its nanostructures show an enormous potential, reaching high QE and promise more robustness. Operational parameters and the information about its behavior in the injector system are not available at the moment, but they are required for advanced electron beam sources.

A future possibility for improving semiconductor photocathodes is to change the surface composition to stabilize or protect the emission layer. Cs:F:Li[168] or Cs:O:Sb[169] can be used to form a protection layer on GaAs photocathodes. Alternatively, Cs_2Te can also be considered as a protective layer for GaAs as already mentioned in Section 5.3.4.[116,129]

In the last years, detailed studies were carried out to explore the influence of a thin graphene layer on the performance of metals and bi-alkali photocathodes.[170–172] These studies report that both photocathodes have a good compatibility leading to a high crystallinity of the emission layer.[173] The application of two monolayers of graphene achieved the highest QE with a homogenous distribution.[171] Besides graphene as a potential coating, the idea of a boron nitride (BN) or molybdenum sulfide (MoS_2) coating for photocathode arose.[174] Wang *et al.* found out that a monolayer of BN maintains the QE, making it an ideal coating material for alkali-based semiconducting photocathodes. This study additionally considered a few layers of graphene or MoS_2 as a useful protection layer but with the disadvantage that those coatings increase the work function of the alkali-based photocathode.

The new avenues opened by the above mentioned coating techniques contribute to the future development of photocathode materials. Simulations and advanced analytical chemistry are necessary to understand the physics and chemistry of the coated photocathodes to guarantee a fabrication of high performance photocathodes for future electron-beam applications.

The improving crystal quality, the optimization of growth conditions and the application of new low-dimensional materials, such as 2D sheets, nanowires and nanotubes push the development of semiconductor photocathodes towards their application in high power devices, detectors and electron source in particle accelerators.

Conflicts of interest

There are no conflicts to declare.

Acknowledgements

This research did not receive any specific grant from funding agencies in the public, commercial, or not-for-profit sectors. The authors would like to thank P. Michel and the ELBE team, especially the SRF Gun group for their support. Special thanks goes to all who proofread the manuscript.

References

1 M. Krysztof, *Microsyst. Nanoeng.*, 2021, **7**, 00268.
2 P. W. Hawkes and J. C. Spence, *Science of Microscopy*, Springer, 2007, vol. 1.
3 L. Zhao, J. Wu, Z. Wang, H. Tang, X. Zou, T. Jiang, P. Zhu, D. Xiang and J. Zhang, *Struct. Dyn.*, 2021, 044303.
4 J. F. Dawson, A. C. Marvin and C. A. Marshman, *Electromagnetic Compatibility*, Encycl. Phys. Sci. Technol., 2003, vol. 3, pp. 261–275.

Open Access Article. Published on 17 2023. Downloaded on 05.11.2024 09:24:16.
This article is licensed under a Creative Commons Attribution-NonCommercial 3.0 Unported Licence.

5 G. Gaertner, W. Knapp and R. G. Forbes, *Modern Developments in Vacuum Electron Sources*, Springer, 2020.
6 S. V. Kutsaev, *Tech. Phys.*, 2021, **66**, 161–195.
7 T. Rao and D. H. Dowell, *An Engineering Guide to Photoinjectors*, Createspace Independent Publishing Platform, 2013.
8 A. T. Odularu, *J. Spectrosc.*, 2020, 8868713.
9 A. T. Khotbeh-sara, F. Rahmani and F. Ghasemi, *Radiat. Phys. Eng.*, 2021, **2**, 9–17.
10 A. G. Kazakov, T. Y. Ekatova and J. S. Babenya, *J. Radioanal. Nucl. Chem.*, 2021, **328**, 493–505.
11 E. Sobolev, S. Zolotarev and K. Giewekemeyer, *Commun. Phys.*, 2020, **3**, 0362.
12 D. Khakhulin, F. Otte, M. Biednov, C. Bömer, T. K. Choi, M. Diez, A. Galler, Y. Jiang, K. Kubicek, F. A. Lima, A. Rodriguez-Fernandez, P. Zalden, W. Gawelda and C. Bressler, *Appl. Sci.*, 2020, **10**, 995.
13 S. Kovalev, K. J. Tielrooij, J. C. Deinert, I. Ilyakov, N. Awari, M. Chen, A. Ponomaryov, M. Bawatna, T. V. de Oliveira, L. M. Eng, K. A. Kuznetsov, D. A. Safronenkov, G. K. Kitaeva, P. I. Kuznetsov, H. A. Hafez, D. Turchinovich and M. Gensch, *npj Quantum Mater.*, 2021, **6**, 84.
14 S. V. Baryshev, E. Wang, C. Jing, V. Jabotinski, S. Antipov, A. D. Kanareykin, S. Belomestnykh, I. Ben-Zvi, L. Chen, Q. Wu, H. Li and A. V. Sumant, *Appl. Phys. Lett.*, 2021, **118**, 053505.
15 L. Cultrera, E. Rocco, F. Shahedipour-Sandvik, L. D. Bell, J. K. Bae, I. V. Bazarov, P. Saha, S. Karkare and A. Arjunan, *J. Appl. Phys.*, 2022, **131**, 124902.
16 P. Tripathi, A. Kumar, S. Dwivedi and P. K. Jain, *IEEE Trans. Plasma Sci.*, 2020, **48**, 438–445.
17 B. Dunham, J. Barley, A. Bartnik, I. Bazarov, L. Cultrera, J. Dobbins, G. Hoffstaetter, B. Johnson, R. Kaplan, S. Karkare, V. Kostroun, Y. Li, M. Liepe, X. Liu, F. Loehl, J. Maxson, P. Quigley, J. Reilly, D. Rice, D. Sabol, E. Smith, K. Smolenski, M. Tigner, V. Vesherevich, D. Widger and Z. Zhao, *Appl. Phys. Lett.*, 2013, **102**, 98–102.
18 O. Tanaka, T. Miyajima and N. Higashi, *Proc. IPAC2021*, 2021, pp. 4531–4534.
19 F. Hug, K. Aulenbacher, S. Friederich, P. Heil, R. G. Heine, R. Kempf, C. Matejcek and D. Simon, 63th ICFA Adv. Beam Dyn. Energy Recover, Linacs, ERL2019, Berlin, 2021, pp. 14-17.
20 A. Lueangaramwong, X. Li, P. Boonpornprasert, O. Lishilin, M. Krasilnikov, Z. Aboulbanine, G. Adhikari, N. Aftab, N. Chaisueb, G. Georgiev, J. Good, M. Gross, C. Koschitzki, D. Melkumyan, H. Qian, G. Shu, G. Vashchenko, T. Weilbach, F. Stephan, D. Zeuthen and H. Shaker, Proc. of 12th Int. Part. Acc. Conf. 2021 (IPAC2021), 2021, pp. 3285-3288.
21 Y. D. Kluchevskaia and S. M. Polozov, *Cybern. Phys.*, 2020, **9**, 98–102.
22 C. C. Xiao, J. Q. Zhang, J. H. Tan and W. C. Fang, *Nucl. Sci. Technol.*, 2020, **31**, 100.
23 R. Xiang, A. Arnold, P. Michel, P. Murcek, J. Teichert, P. Lu and H. Vennekate, IPAC 2014 Proc. 5th Int. Part. Accel. Conf., 2014, pp. 642-644.
24 I. Petrushina, V. N. Litvinenko, Y. Jing, J. Ma, I. Pinayev, K. Shih, G. Wang, Y. H. Wu, Z. Altinbas, J. C. Brutus, S. Belomestnykh, A. Di Lieto, P. Inacker, J. Jamilkowski, G. Mahler, M. Mapes, T. Miller, G. Narayan, M. Paniccia, T. Roser, F. Severino, J. Skaritka, L. Smart, K. Smith, V. Soria, Y. Than, J. Tuozzolo, E. Wang, B. Xiao, T. Xin, I. Ben-Zvi, C. Boulware, T. Grimm, K. Mihara, D. Kayran and T. Rao, *Phys. Rev. Lett.*, 2020, **124**, 244801.
25 D. H. Dowell, I. Bazarov, B. Dunham, K. Harkay, C. Hernandez-Garcia, R. Legg, H. Padmore, T. Rao, J. Smedley and W. Wan, *Nucl. Instrum. Methods Phys. Res., Sect. A*, 2010, **622**, 685–697.
26 F. Hug, K. Aulenbacher, D. Simon, C. P. Stoll and S. D. W. Thomas, 63th ICFA Adv. Beam Dyn. Energy Recover, Linacs, ERL2019, Berlin, 2020, pp. 28-33.
27 Z. T. Zhao, Z. Wang, C. Feng, S. Chen and L. Cao, *Sci. Rep.*, 2021, **11**, 23875.
28 N. Nishimori, I. Bazarov and B. Dunham, *Proc. ERL09*, 2009, pp. 6–23.
29 J. Teichert, A. Arnold, G. Ciovati, J.-C. Deinert, P. Evtushenko, M. Justus, P. Kneisel, S. Kovalev, M. Kuntzsch, U. Lehnert, P. Lu, S. Ma, P. Murcek, P. Michel, A. Ryzhov, J. Schaber, C. Schneider, R. Schurig, R. Steinbrück, H. Vennekate, I. Will and R. Xiang, *Phys. Rev. Accel. Beams*, 2021, **24**, 033401.
30 I. V. Bazarov, B. M. Dunham, X. Liu, M. Virgo, A. M. Dabiran, F. Hannon and H. Sayed, *J. Appl. Phys.*, 2009, **105**, 0837151.
31 R. Xiang and J. Teichert, Phys. Procedia, Int. Conf. Laser Appl. Accel. (LA3NET) 2015, 2015, pp. 58-65.
32 A. Kahn, *Mater. Horiz.*, 2016, **3**, 7–10.
33 D. H. Dowell and J. F. Schmerge, *Phys. Rev. Spec. Top. – Accel. Beams*, 2009, **12**, 074201.
34 G. Gevorkyan, S. Karkare, S. Emamian, I. V. Bazarov and H. A. Padmore, *Phys. Rev. Accel. Beams*, 2018, **21**, 093401.
35 S. Karkare and I. Bazarov, *Phys. Rev. Appl.*, 2015, **4**, 024015.
36 A. Galdi, J. Balajka, W. J. DeBenedetti, L. Cultrera, I. V. Bazarov, M. A. Hines and J. M. Maxson, *Appl. Phys. Lett.*, 2021, **118**, 244101.
37 S. Matsuba, Y. Honda, X. Jin, T. Miyajima, M. Yamamoto, T. Uchiyama, M. Kuwahara and Y. Takeda, *Jpn. J. Appl. Phys.*, 2012, **51**, 046402.
38 P. W. Huang, W. H. Huang and C. X. Tang, Proc. 38th Int. Free. Laser Conf. (FEL 2017), 2017, pp. 394-396.
39 D. H. Dowell, F. K. King, R. E. Kirby, J. F. Schmerge and J. M. Smedley, *Phys. Rev. Spec. Top. – Accel. Beams*, 2006, **9**, 063502.
40 A. di Bona, F. Sabary, S. Valeri, P. Michelato, D. Sertore and G. Suberlucq, *J. Appl. Phys.*, 1998, **80**, 3024.
41 H. Iijima, M. Kuriki and Y. Masumoto, 2nd Int. Part. Accel. Conf. 2011 (IPAC 2011), 2011, pp. 3158-3160.
42 D. K. Schroder, N. R. Thomas, J. Vine and H. Nathanson, *Trans. Electron Dev.*, 1974, **21**, 785–798.
43 J. Shao, J. Shi, S. P. Antipov, S. V. Baryshev, H. Chen, M. Conde, W. Gai, G. Ha, C. Jing, F. Wang and E. Wisniewski, *Phys. Rev. Lett.*, 2016, **117**, 084801.

Open Access Article. Published on 17 2023. Downloaded on 05.11.2024 09:24:16.
This article is licensed under a Creative Commons Attribution-NonCommercial 3.0 Unported Licence.

44 D. Sertore, S. Schreiber, K. Floettmann, F. Stephan, K. Zapfe and P. Michelato, *Nucl. Instrum. Methods Phys. Res., Sect. A*, 2000, **445**, 422–426.

45 J. H. Han, J. Bähr, H. J. Grabosch, M. Krasilnikov, V. Miltchev, A. Oppelt, B. Petrosyan, S. Riemann, L. Staykov, F. Stephan, M. V. Hartrott, K. Flöttmann, S. Schreiber, J. Rönsch, P. Michelato, L. Monaco and D. Sertore, Proc. of IEEE Part. Accel. Conf., 2005, pp. 895-897.

46 A. Aryshev, M. Shevelev, Y. Honda, N. Terunuma and J. Urakawa, *Appl. Phys. Lett.*, 2017, **111**, 033508.

47 L. Cultrera, I. Bazarov, A. Bartnik, B. Dunham, S. Karkare, R. Merluzzi and M. Nichols, *Appl. Phys. Lett.*, 2011, **99**, 152110.

48 L. Cultrera, J. Maxson and I. Bazarov, *Phys. Rev. ST Accel. Beams*, 2011, **14**, 120101.

49 C. Hernandez-Garcia, B. Bullard, J. Benesch, J. Grames, J. Gubeli, F. Hannon, J. Hansknecht, J. Jordan, R. Kazimi, G. A. Krafft, M. A. Mamun, M. Poelker, M. L. Stutzman, R. Suleiman, M. Tiefenback, Y. Wang, S. Zhang, C. A. Valerio Lizarraga, R. Montoya Soto and A. Canales Ramos, *Phys. Rev. Accel. Beams*, 2019, **22**, 113401.

50 R. Xiang, A. Arnold, P. Lu, P. Murcek, J. Teichert and H. Vennekate, Proc. of IPAC 2018, 2018, pp. 4142-4144.

51 E. Wang, V. N. Litvinenko, I. Pinayev, M. Gaowei, J. Skaritka, S. Belomestnykh, I. Ben-Zvi, J. C. Brutus, Y. Jing, J. Biswas, J. Ma, G. Narayan, I. Petrushina, O. Rahman, T. Xin, T. Rao, F. Severino, K. Shih, K. Smith, G. Wang and Y. Wu, *Sci. Rep.*, 2021, **11**, 4477.

52 Y. Zhou and P. Zhang, *J. Appl. Phys.*, 2020, **127**, 164903.

53 W. E. Spicer, *Phys. Rev.*, 1958, **112**, 114.

54 S. Karkare, D. Dimitrov, W. Schaff, L. Cultrera, A. Bartnik, X. Liu, E. Sawyer, T. Esposito and I. Bazarov, *J. Appl. Phys.*, 2013, **113**, 104904.

55 X. Y. Wu, H. Liang, M. F. Ciappina and L. Y. Peng, *Photonics*, 2020, **7**, 129.

56 O. Chubenko, S. Karkare, D. A. Dimitrov, J. K. Bae, L. Cultrera, I. Bazarov and A. Afanasev, *J. Appl. Phys.*, 2021, **130**, 063101.

57 Z. Jiang, Q. Gu, X. Li, E. Wang, M. Gaowei and W. Liu, *Phys. Rev. Accel. Beams*, 2021, **24**, 33402.

58 E. R. Antoniuk, Y. Yue, Y. Zhou, P. Schindler, W. A. Schroeder, B. Dunham, P. Pianetta, T. Vecchione and E. J. Reed, *Phys. Rev. B*, 2020, **101**, 235447.

59 C. Metzger, M. Graus, M. Grimm, G. Zamborlini, V. Feyer, M. Schwendt, D. Lüftner, P. Puschnig, A. Schöll and F. Reinert, *Phys. Rev. B*, 2020, **101**, 165421.

60 R. Amador and H.-d Saßnick, *J. Phys.: Condens. Matter*, 2021, **33**, 365502.

61 J. Krumland, A. M. Valencia, S. Pittalis, C. A. Rozzi and C. Cocchi, *J. Chem. Phys.*, 2020, **153**, 054106.

62 H.-D. Saßnick and C. Cocchi, *Electron. Struct.*, 2021, **3**, 027001.

63 R. P. Xian, V. Stimper, M. Zacharias, S. Dong, M. Dendzik, S. Beaulieu, B. Schölkopf, M. Wolf, L. Rettig, C. Carbogno, S. Bauer and R. Ernstorfer, *Nat. Comput. Sci.*, 2022, **1**, 00382.

64 J. M. Howard, Q. Wang, E. Lee, R. Lahoti, T. Gong, M. Srivastava, A. Abate and M. S. Leite, *arXiv*, 2020, 03702, DOI: 10.48550/arXiv.2010.03702.

65 J. Westermayr and R. J. Maurer, *Chem. Sci.*, 2021, **12**, 10755–10764.

66 L. Ward, A. Agrawal, A. Choudhary and C. Wolverton, *npj Comput. Mater.*, 2016, **2**, 16028.

67 A. Talapatra, B. P. Uberuaga, C. R. Stanek and G. Pilania, *Chem. Mater.*, 2021, **33**, 845–858.

68 H. C. Wang, S. Botti and M. A. Marques, *npj Comput. Mater.*, 2021, **7**, 00481.

69 Y. Zhang, K. Zhang, S. Li, S. Li, Y. Qian, F. Shi, G. Jiao, Z. Miao, Y. Guo and Y. Zeng, *J. Appl. Phys.*, 2020, **128**, 173103.

70 F. Machuca, Z. Liu, Y. Sun, P. Pianetta, W. E. Spicer and R. F. W. Pease, *J. Vac. Sci. Technol., B: Nanotechnol. Microelectron.: Mater., Process., Meas., Phenom.*, 2003, **21**, 1863.

71 C. I. Wu and A. Kahn, *J. Appl. Phys.*, 1999, **86**, 3209–3212.

72 J. Kühn, M. Bürger, A. Frahm, A. Jankowiak, T. Kamps, G. Klemz, G. Kourkafas, P. Murcek, A. Neumann, N. Ohm, M. Schmeißer, M. Schuster, J. Teichert and J. Völker, Proc. of IPAC2018, 2018, pp. 1247-1250.

73 L. B. Jones, D. P. Juarez-Lopez, B. L. Militsyn, C. P. Welsch and T. C. Q. Noakes, Proc. IPAC2018, 2018, pp. 4438-4441.

74 J. Smedley, T. Rao and J. Sekutowicz, *Phys. Rev. Spec. Top. – Accel. Beams*, 2008, **11**, 013502.

75 B. Feuerbacher and B. Fitton, *J. Appl. Phys.*, 1972, **43**, 1563–1572.

76 A. A. Turnbull and G. B. Evans, *J. Phys. D: Appl. Phys.*, 1968, **1**, 155–160.

77 C. P. Hauri, R. Ganter, F. Le Pimpec, A. Trisorio, C. Ruchert and H. H. Braun, *Phys. Rev. Lett.*, 2010, **104**, 234802.

78 H. J. Qian, J. B. Murphy, Y. Shen, C. X. Tang and X. J. Wang, *Appl. Phys. Lett.*, 2010, **97**, 1–4.

79 H. J. Qian, C. Li, Y. C. Du, L. X. Yan, J. F. Hua, W. H. Huang and C. X. Tang, *Phys. Rev. Spec. Top. – Accel. Beams*, 2012, **15**, 040102.

80 H. B. Michaelson, *J. Appl. Phys.*, 1977, **48**, 4729–4733.

81 L. A. J. Soomary, D. P. Juarez-Lopez, C. P. Welsch, L. B. Jones and T. C. Q. Noakes, Proc. of IPAC2021, 2021, pp. 2860-2862.

82 S. Karkare, G. Adhikari, W. A. Schroeder, J. K. Nangoi, T. Arias, J. Maxson and H. Padmore, *Phys. Rev. Lett.*, 2020, **125**, 54801.

83 P. Michelato, Proc. of EPAC08, 2008, pp. 46-50.

84 S. H. Kong, J. Kinross-Wright, D. C. Nguyen and R. L. Sheffield, *Nucl. Instrum. Methods Phys. Res., Sect. A*, 1995, **358**, 272–275.

85 G. Suberlucq, Proc. of EPAC 2004, 2004, p. 602.

86 Z. Yusof, A. Denchfield, M. Warren, J. Cardenas, N. Samuelson, L. Spentzouris, J. Power and J. Zasadzinski, *Phys. Rev. Accel. Beams*, 2017, **20**, 123401.

87 S. H. Kong, J. Kinross-Wright, D. C. Nguyen and R. L. Sheffield, *J. Appl. Phys.*, 1995, **77**, 6031–6038.

88 S. Ledere, J. H. Han, S. Schreiber, A. Vollmer, R. Ovsyannikov, M. Sperling, H. Duerr, F. Stephan, P. Michelato, L. Monaco, C. Pagani and D. Sertore, 29th

Open Access Article. Published on 17 2023. Downloaded on 05.11.2024 09:24:16.
This article is licensed under a Creative Commons Attribution-NonCommercial 3.0 Unported Licence.

Int. Free Electron Laser Conf. 2007 (FEL 2007), 2007, pp. 457-460.

89 S. Lederer, S. Schreiber, P. Michelato, C. Pagani, D. Sertore, L. Monaco and J. Han, Proc. of EPAC08, 2008, pp. 232-234.

90 S. Lederer, F. Brinker and S. Schreiber, Proc. 39th Int. Free. Laser Conf. 2019 (FEL 2019), 2019, pp. 427-429.

91 L. Monaco, P. Michelato, D. Sertore, C. Pagani and G. Guerini Rocco, Proc. of 39th Int. Free. Laser Conf. 2019 (FEL 2019), 2019, pp. 297-300.

92 P. Huang, H. Qian, Y. Chen, A. Grigoryan, M. Gross, I. Isaev, P. Kitisri, C. Koschitzki, M. Krasilnikov, S. Lal, X. Li, O. Lishilin, D. Melkumyan, R. Niemczyk, A. Oppelt, H. Shaker, G. Shu, F. Stephan, G. Vashchenko, T. Weilbach, S. Lederer, L. Monaco, P. Michelato and D. Sertore, Proc. of 39th Int. Free. Laser Conf. 2019 (FEL 2019), 2019, pp. 473-476.

93 V. Miltchev, J. Baehr, H. J. Grabosch, J. H. Han, M. Krasilnikov, A. Oppelt, B. Petrosyan, L. Staykov, F. Stephan and M. V. Hartrott, Proc. of 27th Int. Free Electron Laser Conf. 2005 (FEL 2005), 2005, pp. 560-563.

94 L. Zheng, J. Shao, E. E. Wisniewski, J. G. Power, Y. Du, W. Liu, C. E. Whiteford, M. Conde, S. Doran, C. Jing and C. Tang, *Phys. Rev. Accel. Beams*, 2020, **23**, 52801.

95 K. Floettmann, *TESLA FEL Rep.*, 1997, **97**, 01.

96 R. Xiang, A. Arnold, P. Michel, P. Murcek and J. Teichert, Proc. of FEL2010, 2010, pp. 449-452.

97 P. W. Huang, H. Qian, Y. Chen and D. Filippetto, *Phys. Rev. Accel. Beams*, 2020, **23**, 43401.

98 F. Zhou, C. Adolphsen, A. Benwell, G. Brown, D. H. Dowell, M. Dunning, S. Gilevich, K. Grouev, G. Huang, B. Jacobson, X. H. Liu, A. Miahnahri, F. Sannibale, J. Schmerge and T. Vecchione, *Phys. Rev. Accel. Beams*, 2021, **24**, 73401.

99 N. Chanlek, J. D. Herbert, R. M. Jones, L. B. Jones, K. J. Middleman and B. L. Militsyn, *J. Phys. D: Appl. Phys.*, 2015, **48**, 375102.

100 G. Loisch, Y. Chen, C. Koschitzki, H. Qian, M. Gross, A. Hannah, A. Hoffmann, D. Kalantaryan, M. Krasilnikov, S. Lederer, X. Li, O. Lishilin, D. Melkumyan, L. Monaco, R. Niemczyk, A. Oppelt, D. Sertore, F. Stephan, R. Valizadeh, G. Vashchenko and T. Weilbach, *Appl. Phys. Lett.*, 2022, **120**, 104101.

101 R. Xiang, A. Arnold, H. Buettig, D. Janssen, M. Justus, U. Lehnert, P. Michel, P. Murcek, A. Schamlott, C. Schneider, R. Schurig, F. Staufenbiel and J. Teichert, *Phys. Rev. Spec. Top. – Accel. Beams*, 2010, **13**, 043501.

102 S. Schreiber, S. Lederer, L. Monaco, D. Sertore and P. Michelato, Proc. of 38th Int. Free. Laser Conf. 2017 (FEL 2017), 2017, pp. 415-418.

103 A. H. Sommer, *Rev. Sci. Instrum.*, 1955, **26**, 725–726.

104 M. A. Schmeißer, S. Mistry, H. Kirschner, S. Schubert, A. Jankowiak, T. Kamps and J. Kühn, *Phys. Rev. Accel. Beams*, 2018, **21**, 113401.

105 D. H. Dowell, K. J. Davis, K. D. Friddell, E. L. Tyson, C. A. Lancaster, L. Milliman, R. E. Rodenburg, T. Aas, M. Bemes, S. Z. Bethel, P. E. Johnson, K. Murphy, C. Whelen, G. E. Busch and D. K. Remelius, *Appl. Phys. Lett.*, 1993, **63**, 2035–2037.

106 I. Bazarov, L. Cultrera, A. Bartnik, B. Dunham, S. Karkare, Y. Li, X. Liu, J. Maxson and W. Roussel, *Appl. Phys. Lett.*, 2011, **98**, 224101.

107 Y. Wang, M. A. Mamun, P. Adderley, B. Bullard, J. Grames, J. Hansknecht, C. Hernandez-Garcia, R. Kazimi, G. A. Krafft, G. Palacios-Serrano, M. Poelker, M. L. Stutzman, R. Suleiman, M. Tiefenback, S. Wijethunga, J. Yoskowitz and S. Zhang, *Phys. Rev. Accel. Beams*, 2020, **23**, 103401.

108 X. Wang, Y. Zhang, H. Yu and J. Wu, *Optik*, 2016, **127**, 7611–7624.

109 J. Ma, X. Fu, M. Yang, H. Zhao and S. Ren, Proc. of IEEE 4th Adv. Inf. Technol. Electron. Autom. Control Conf. 2019 (IAEAC 2019), 2019, pp. 1451-1455.

110 J. J. Scheer and J. V. Laar, *Solid State Commun.*, 1965, **3**, 189–193.

111 X. Zhu, F. Lin, Z. Zhang, X. Chen, H. Huang, D. Wang, J. Tang, X. Fang, D. Fang, J. C. Ho, L. Liao and Z. Wei, *ACS Appl. Mater. Interfaces*, 2020, **20**, 2654–2659.

112 M. Kuwahara, S. Kusunoki, Y. Nambo, K. Saitoh, X. Jin, T. Ujihara, H. Asano, Y. Takeda and N. Tanaka, *Appl. Phys. Lett.*, 2014, **105**, 193101.

113 L. Liu, Y. Diao and S. Xia, *J. Mater. Sci.*, 2019, **54**, 5605–5614.

114 G. L. Carr, M. C. Martin, W. R. McKinney, K. Jordan, G. R. Neil and G. P. Williams, *Nature*, 2002, **420**, 153–156.

115 N. Scahill and K. Aulenbacher, *J. Appl. Phys.*, 2022, **132**, 185702.

116 J. Biswas, E. Wang, M. Gaowei, W. Liu, O. Rahman and J. T. Sadowski, *AIP Adv.*, 2021, **11**, 025321.

117 A. Özkartal and D. T. Noori, *J. Mater. Sci.: Mater. Electron.*, 2021, **32**, 13462–13471.

118 I. Levchenko, V. Tomashyk, G. Malanych, I. Stratiychuk and A. Korchovyi, *Appl. Nanosci.*, 2021, **12**, 1139–1145.

119 Y. Zhang, C. Fang, Y. Qian, J. Zhang, K. Zhang, J. Zhang, M. Rong, F. Shi, G. Jiao and X. Bai, *Proc. SPIE*, 2020, p. 54.

120 N. Razek, K. Otte, T. Chassé, D. Hirsch, A. Schindler, F. Frost and B. Rauschenbach, *J. Vac. Sci. Technol., A*, 2002, **20**, 1492–1497.

121 G. Greczynski and L. Hultman, *Appl. Surf. Sci.*, 2021, **542**, 148599.

122 K. Togawa, T. Nakanishi, T. Baba, F. Furuta, H. Horinaka, T. Ida, Y. Kurihara, H. Matsumoto, T. Matsuyama, M. Mizuta, S. Okumi, T. Omori, C. Suzuki, Y. Takeuchi, K. Wada, K. Wada and M. Yoshioka, *Nucl. Instrum. Methods Phys. Res., Sect. A*, 1998, **414**, 431–445.

123 B. S. Henderson, *Study of Negative Electron Affinity GaAs Photocathodes*, Rice university, technical report, 2009.

124 D. G. Fisher, R. E. Enstrom, J. S. Escher and B. F. Williams, *J. Appl. Phys.*, 1972, **43**, 3815–3823.

125 D. Sato, T. Nishitani, Y. Honda and H. Amano, *J. Vac. Sci. Technol., B*, 2020, **38**, 012603.

126 S. Pastuszka, M. Hoppe, D. Kratzmann, D. Schwalm, A. Wolf, A. S. Jaroshevich, S. N. Kosolobov, D. A. Orlov and A. S. Terekhov, *J. Appl. Phys.*, 2000, **88**, 6788–6800.

127 C. Feng, Y. Zhang, J. Liu, Y. Qian, J. Zhang, J. Zhao, F. Shi and X. Bai, *Mater. Sci. Semicond. Process.*, 2019, **91**, 41–46.

 This journal is © The Royal Society of Chemistry 2023

Open Access Article. Published on 17 2023. Downloaded on 05.11.2024 09:24:16.
This article is licensed under a Creative Commons Attribution-NonCommercial 3.0 Unported Licence.

128 D. T. Pierce, R. J. Celotta, G. C. Wang, W. N. Unertl, A. Galejs, C. E. Kuyatt and S. R. Mielczarek, *Rev. Sci. Instrum.*, 1980, **51**, 478–499.
129 J. K. Bae, A. Galdi, L. Cultrera, F. Ikponmwen, J. Maxson and I. Bazarov, *J. Appl. Phys.*, 2020, **127**, 124901.
130 N. Yamamoto, M. Yamamoto, M. Kuwahara, R. Sakai, T. Morino, K. Tamagaki, A. Mano, A. Utsu, S. Okumi, T. Nakanishi, M. Kuriki, C. Bo, T. Ujihara and Y. Takeda, *J. Appl. Phys.*, 2007, **102**, 024904.
131 Y. Zhang and G. Jiao, *Adv. Photodetectors – Res. Appl.*, IntechOpen, 2018, ch. 4, p. 80704.
132 L. Cultrera, A. Galdi, J. K. Bae, F. Ikponmwen, J. Maxson and I. Bazarov, *Phys. Rev. Accel. Beams*, 2020, **23**, 23401.
133 J. K. Bae, L. Cultrera, P. Digiacomo and I. Bazarov, *Appl. Phys. Lett.*, 2018, **112**, 1–6.
134 E. Wang, J. Kewisch, A. Burrill, T. Rao, Q. Wu and D. Holmes, Proc. of Part. Accel. Conf. (IPAC 2011), 2011.
135 D. T. Pierce, R. J. Celotta, G. C. Wang, W. N. Unertl, A. Galejs, C. E. Kuyatt and S. R. Mielczarek, *Rev. Sci. Instrum.*, 1980, **51**, 478–499.
136 J. L. McCarter, N. B. Clayburn, J. M. Dreiling, T. J. Gay, D. M. Ryan, J. Hansknecht, M. Poelker, A. Afanasev and A. Kechiantz, Proc. of 15th International Workshop on Polarized Sources, Targets, and Polarimetry 2013 (PSTP 2013), 2013, p. 060.
137 W. Liu, M. Poelker, X. Peng, S. Zhang and M. Stutzman, *J. Appl. Phys.*, 2017, **122**, 035703.
138 T. Maruyama, A. Brachmann, J. E. Clendenin, T. Desikan, E. L. Garwin, R. E. Kirby, D. A. Luh, J. Turner and R. Prepost, *Nucl. Instrum. Methods Phys. Res., Sect. A*, 2002, **492**, 199–211.
139 W. Liu, Y. Chen, W. Lu, A. Moy, M. Poelker, M. Stutzman and S. Zhang, *Appl. Phys. Lett.*, 2016, **109**, 252104.
140 A. Prabaswara, J. Birch, M. Junaid, E. A. Serban, L. Hultman and C. L. Hsiao, *Appl. Sci.*, 2020, **10**, 3050.
141 F. Machuca, Y. Sun, Z. Liu, K. Ioakeimidi, P. Pianetta and R. F. W. Pease, *J. Vac. Sci. Technol., B*, 2000, **18**, 3042.
142 X. Wang, M. Wang, Y. Liao, L. Yang, Q. Ban, X. Zhang, Z. Wang and S. Zhang, *J. Mater. Chem. C*, 2021, **9**, 13013–13040.
143 S. Uchiyama, Y. Takagi, M. Niigaki, H. Kan and H. Kondoh, *Appl. Phys. Lett.*, 2005, **86**, 103511.
144 X. Fu, X. Wang, Y. Yang, B. Chang, Y. Du, J. Zhang and R. Fu, *Optik*, 2012, **123**, 765–768.
145 J. Fu, W. Liu, S. Zhang and H. Ma, *Optik*, 2014, **125**, 1485–1487.
146 H. Wang, J. Liu, N. Niu, G. Shen and S. Zhang, *J. Cryst. Growth*, 2007, **304**, 7–10.
147 C. Bayram, J. L. Pau, R. McClintock and M. Razeghi, *J. Appl. Phys.*, 2008, **104**, 083512.
148 A. Jarndal, L. Arivazhagan and D. Nirmal, *Int. J. RF Microw. Comput. Eng*, 2020, **30**, 22196.
149 S. A. Kukushkin, A. V. Osipov, V. N. Bessolov, B. K. Medvedev, V. K. Nevolin and K. A. Tcarik, *Rev. Adv. Mater. Sci.*, 2008, **17**, 1–32.
150 L. Liu, J. Tian, F. Lu, X. Zhangyang and Z. Lv, *Opt. Commun.*, 2020, **475**, 126241.
151 O. Siegmund, J. Vallerga, J. McPhate, J. Malloy, A. Tremsin, A. Martin, M. Ulmer and B. Wessels, *Nucl. Instrum. Methods Phys. Res., Sect. A*, 2006, **567**, 89–92.
152 F. Chen, X. Ji and S. P. Lau, *Mater. Sci. Eng., R*, 2020, **142**, 100578.
153 S. Xia, L. Liu, Y. Diao and Y. Kong, *Opt. Mater.*, 2017, **64**, 187–192.
154 L. Guo, H. Yamaguchi, M. Yamamoto, F. Matsui, G. Wang, F. Liu, P. Yang, E. R. Batista, N. A. Moody, Y. Takashima and M. Katoh, *Appl. Phys. Lett.*, 2020, **116**, 251903.
155 T. Yayama, A. K. A. Lu, T. Morishita and T. Nakanishi, *Appl. Phys. Lett.*, 2021, **119**, 203101.
156 X. Zhang, L. Liu, Z. Lv, F. Lu and J. Tian, *Int. J. Energy Res.*, 2021, **45**, 2265–2276.
157 D. Sato, A. Honda, A. Koizumi, T. Nishitani, Y. Honda and H. Amano, *Microelectron. Eng.*, 2020, **223**, 111229.
158 D. Sato, H. Shikano, A. Koizumi and T. Nishitani, *J. Vac. Sci. Technol., B*, 2022, **40**, 064204.
159 A. Koizumi, D. Sato, H. Shikano, H. Iijima and T. Nishitani, *J. Vac. Sci. Technol., B*, 2022, **40**, 062202.
160 F. Machuca, Z. Liu, Y. Sun, P. Pianetta, W. E. Spicer and R. F. W. Pease, *J. Vac. Sci. Technol., A*, 2002, **20**, 1784–1786.
161 L. L. Smith, S. W. King, R. J. Nemanich and R. F. Davis, *J. Electron. Mater.*, 1996, **25**, 805–810.
162 J. Qiao, S. Wang and D. Huang, *Proc. SPIE*, 2019, vol. 10843, p. 108430I.
163 J. Schaber, R. Xiang, J. Teichert, A. Arnold, P. Murcek, P. Zwartek, A. Ryzhov, S. Ma, S. Gatzmaga, P. Michel and N. Gaponik, *Micromashines*, 2022, **13**, 849.
164 M. Vogel, M. Schumacher and X. Jiang, Proc. of 9th International Particle Accelerator Conference (IPAC 2018), 2018, pp. 4594-4597.
165 L. Liu, F. Lu, J. Tian, X. Zhangyang and Z. Lv, *MRS Commun.*, 2021, **11**, 931–935.
166 L. Velardi, V. Turco, L. Monteduro, G. Cicala, A. Valentini and V. Nassisi, *Phys. Rev. Accel. Beams*, 2019, **22**, 93402.
167 C. An, R. Zhu, J. Xu, Y. Liu and D. Yu, *Phys. Rev. Accel. Beams*, 2021, **24**, 93401.
168 N. Kurichiyanil, J. Enders, Y. Fritzsche and M. Wagner, *J. Instrum.*, 2019, **14**, P08025.
169 J. K. Bae, M. Andorf, A. Bartnik, A. Galdi, L. Cultrera, J. Maxson and I. Bazarov, *AIP Adv.*, 2022, **12**, 095017.
170 F. Liu, L. Guo, J. Defazio, V. Pavlenko, M. Yamamoto, N. A. Moody and H. Yamaguchi, *ACS Appl. Mater. Interfaces*, 2022, **14**, 1710–1717.
171 J. Biswas, M. Gaowei, A. Liu, S. Poddar, L. Stan, J. Smedley, J. T. Sadowski and X. Tong, *APL Mater.*, 2022, **10**, 111115.
172 Y. Zhang, J. Zhan, S. Li, S. Tang, K. Zhang, Z. Wang, Y. Qian, J. Zhang, F. Shi, G. Jiao and L. Yan, *J. Mater. Res. Technol.*, 2022, **21**, 3767–3776.
173 H. Yamaguchi, L. Fangze, J. Defazio, M. Gaowei, V. C. W. Narvaez, X. Junqi, S. John, S. Derek and V. Pavlenko, *Adv. Mater. Interfaces*, 2018, **5**, 1800249.
174 G. Wang, P. Yang, N. A. Moody and E. R. Batista, *npj 2D Mater. Appl.*, 2018, **2**, 0062.